Bridge Damage Detection Using Rotation Measurements – Experimental Validation

F. Huseynov[1, 2], C. Kim[3], E.J. OBrien[2], J.M.W. Brownjohn[1,4], D. Hester[5], K.C Chang[3]

[1] Full Scale Dynamics Ltd., Kay Building North Park Road, Exeter EX4 4QF

[2] School of Civil Engineering, University College Dublin, Richview Newstead Block B, Belfield, Dublin, Ireland

[3]Department of Civil and Earth Resources Engineering, Kyoto University, Kyoto 615-8540, Japan

[4] Vibration Engineering Section, College of Engineering, Mathematics and Physical Sciences, University of Exeter, North Park Road, EX4 4QF Exeter, UK

[5] School of Natural and Built Environment, Queen's University Belfast, Stranmillis Road, BT9 5AG Belfast, Northern Ireland, UK.

Contact author: Farhad Huseynov

Kay Building North Park Road,

Exeter. UK

EX4 6BH

E-mail: f.huseynov@fullscaledynamics.com

Tel: 07533118686

Body text word count:

Number of figures:

Number of tables:

Abstract

This paper presents a novel bridge condition assessment methodology using direct rotation measurements. Initially, numerical analyses are carried out to develop the theoretical basis of the proposed bridge damage detection methodology. As a result of this study the difference in rotation influence lines obtained for healthy and damaged bridge states is proposed as a damage indicator. The sensitivity of rotation to damage and the effect of sensor locations on sensor sensitivities are investigated. Subsequently, extensive laboratory experiments are conducted on a 5.4 m long simply supported bridge structure in an effort to validate the results from the numerical analyses. The test structure is instrumented with rotation sensors and axle detectors and loaded with a four-axle moving vehicle. In this study, rotations are measured using high grade uniaxial accelerometers. The procedure of measuring rotations using accelerometers is explained within the scope of this study. To test the robustness of the proposed bridge condition assessment methodology, a wide range of single and multiple damage scenarios is investigated and the results from this study show that the proposed methodology can successfully identify damage on a bridge. For the model considered, damage as low as 7% change in stiffness over an extent of 2.5% bridge span is shown to be detectable.

1   Introduction

While the bridge stock around the world is aging, the demand put on transportation infrastructure is continuously increasing, making it, in many cases, kept in service longer than it is originally designed for. According to a recent investigation by the RAC foundation, the number of substandard council-maintained road bridges in the UK has risen 35% in just two years [1] and the resulting cost of clearing the backlog of work associated with the deterioration of the country's bridge stock is estimated to be £5 billion. These substandard bridges do not only have a great impact on the economy but are also a threat to public safety. Hence, identifying possible structural defects on a bridge at an early stage is important to prevent unexpected maintenance needs and is the main motivation behind this study.

Bridge condition monitoring systems are broadly categorised in four levels, based on the information they are capable of providing [2].

- Level – I: Identifying the presence of damage
- Level – II: Detecting the presence of damage and its location
- Level – III: Quantifying the severity of damage and its location
- Level – IV: Quantifying the reserve capacity of the structure

This paper proposes a Level-II bridge condition monitoring methodology using the bridge rotation response to a moving load to identify damage in a bridge. Like vertical translation, rotation is a parameter that is sensitive to damage, but rotation is typically easier to measure. To give context to this work, Section 1.1 gives a brief overview of bridge condition monitoring systems using the response of a structure to a moving force, Section 1.2 reviews bridge monitoring case studies where rotation sensors (inclinometers / tiltmeters) have been installed on bridges previously and Section 1.3 describes the objectives of the study.

1.1 Existing bridge damage detection approaches using the response of a bridge to a moving load.

In recent years many authors have placed emphasis upon identifying localised damage in a bridge from its response to a moving load. Some authors use a wavelet transform of beam translation [3, 4] or acceleration [5] response to a moving vehicle to identify damage in a beam, while other researchers have applied empirical mode decomposition to the acceleration response [6, 7]. Most of these methodologies identify damage through the identification of a anomaly in a processed signal for the damaged bridge state which is not present for the healthy condition. In [8], Gonzalez and Hester investigate the damage anomaly in an acceleration response by dividing it into three components: static, dynamic and damage components and demonstrate that the location of the damage relative to the sensor location has a significant impact on the amplitude of the anomaly. He and Zhu [9] investigate the dynamic response of a simply supported beam as a combination of two components; namely, the moving-frequency and the natural-frequency components and develops a simple damage localization approach using a discrete wavelet transform. The method is time saving and easy to implement as it utilises single sensor measurements.

In [10], the authors use an indirect approach; they apply a Moving Force Identification algorithm to the translation response and use the calculated force histories as indicators of bridge damage. In another indirect approach, Li and Au [11] calculate the modal strain energy of the acceleration signals from multiple vehicle passes and succeed in localising damage from the extracted frequencies of healthy and damaged bridges. Others use strain response in a bridge to ambient traffic and identify damage from a change in the position of the neutral axis of the main girders or a change in the transverse load distribution factors [12–15]. In [16] the authors develop a novel damage localization technique for a long suspension bridge based on stress influence lines (SILs) obtained using strain responses of a bridge to traversing vehicles. As a result of

4

this study, three damage indices are proposed based on the derived SIL, namely, the change in SIL and its first order and second order derivatives. The results from the comparative study of damage scenarios show that the first-order derivatives of SIL damage index is the best among the three proposed indices. However, the proposed methodology is found to be effective only for localisation of severe damage scenarios.

1.2 Overview of bridge damage detection methods using direct rotation measurements

Inclinometers (rotation sensors) are designed to measure angular rotation of a test specimen with respect to an 'artificial horizon'. The main operating principle of most commercially available inclinometers is that they perform measurements of different types of response generated by pendulum behaviour due to gravity. The types of pendulum used in inclinometer sensors can be categorized as solid mass [17], liquid [18] and gas [19] [20], and these are measured using resistive [21], capacitive [22], inductive [23], magnetic [24], fibre optic [25] or optical [26] methods.

Inclinometers have been widely utilized in industrial applications such as automotive, aerospace and electronics. Early examples of inclinometers used in the civil engineering industry are seen in geotechnical applications due to inherently greater magnitudes of movements. However, in the last decade, the performance and accuracy of inclinometers has been significantly improved which has made them suitable for bridge SHM applications. Table 1 summarises the technical specifications for some of the commercially available inclinometers. It is now possible to measure tiny rotations, inherent in bridge structures, to 3.5×10^{-4} degree accuracy using state-of-the-art sensors [27–30]. However, as shown in the table, a sensor with a better accuracy has a lower data sampling frequency. Nevertheless, the high accuracy that is achievable using the rotation sensors is part of the motivation behind carrying out the current study to see if they can be used for damage detection purposes.

5

Table 1. Technical specifications of commercially available inclinometers

Model	Manufacturer	Country of Origin	Measurement Range	Precision in degrees	Resolution in degrees	Sampling Rate
HI-INC	Bean Air	Germany	$\pm 15°$	$\pm 5 \times 10^{-2}°$	$1 \times 10^{-3}°$	100 Hz
DNS	MP SENSOR	Germany	$\pm 85°$	$\pm 3 \times 10^{-2}°$	$3 \times 10^{-3}°$	100 Hz
JDI 100	Jewell Instruments	U.S.A	$\pm 1°$	$\pm 4 \times 10^{-3}°$	$1 \times 10^{-4}°$	125 Hz
JN2101	IFM Electronic	Germany	$\pm 45°$	$\pm 1 \times 10^{-2}°$	$1 \times 10^{-3}°$	20 Hz
ACA2200	RION	Japan	$\pm 0.5°$	$\pm 3 \times 10^{-3}°$	$1 \times 10^{-4}°$	20 Hz
ZERO-TRONIC	WYLER AG	Switzerland	$\pm 0.5°$	$\pm 3.5 \times 10^{-4}°$	$1 \times 10^{-4}°$	10 Hz
T935	Sherborne Sensors	U.K	$\pm 1°$	$\pm 4 \times 10^{-4}°$	$6 \times 10^{-5}°$	10 Hz

Inclinometers have been utilised in bridge structures to better understand their complex structural behaviour during the construction and / or operational stages. Glišić et al. [31] monitored a curved concrete post-tensioned bridge during its construction, post-tensioning and first year of service life period using long-gauge deformation sensors and inclinometers. The results helped to verify the post-tensioning and the sound performance of the bridge during its first year of service life. Others monitored rotations on long-span cable supported and suspension bridge structures to better understand their long term performance [32–35]. In [36–38], researchers installed inclinometers at the supports of the test bridge to investigate the boundary conditions.

Inclinometers have also been used to calculate the deformed shape of a bridge deck [39–48]. The advantage over other methods of measuring bridge deflections is that these

techniques do not require a reference point, i.e., they are inertial. Several researchers have also proposed techniques of obtaining bridge modal properties utilizing inclinometers [49, 50].

Although bridge monitoring techniques using inclinometers have been proven to be useful for understanding structural behaviour, there is a limited number of studies in the literature on the use of direct rotation measurement for the identification of damage in a bridge. This is likely to be due to the limitations in the sensor technology. i.e. lack of accurate commercially available sensors as well as sampling rate limitations. The only bridge damage detection techniques that authors could find are proposed in [51, 52]. In one of only two studies found, Alten et al. [51] conducted a progressive damage case study on an aging bridge to evaluate different bridge condition assessment techniques. The test bridge was monitored over 12 weeks using accelerometers, inclinometers and strain sensors while it underwent three damage scenarios. Acceleration data was used to identify damage through changes in modal frequencies whereas the effect of damage on strain and rotation data was investigated by examining the increase in the magnitude of measurements. In this study, the bridge assessment methodology using inclinometers was found to be the most effective. On the other hand, the methodology of identifying damage from changes in modal parameters failed to identify all three damage scenarios, and only the strain sensors installed close to damage locations demonstrated slight increases in strain measurements. In contrast, the effect of damage was clearly evident in rotation measurements at all channels for all three damage scenarios. In the other example of damage identification [52], researchers investigated the sensitivity of rotation to damage in a bridge through numerical and experimental analyses. They proposed a bridge damage detection method referred to as Deformation Area Difference (DAD) that identifies damage from the difference in area between the rotation diagrams obtained for healthy and damaged bridge states under static loading. It is shown in the

7

study that when damage occurs, it results in an increase in DAD factors and the maximum peak occurs at the damage location. However, the disadvantage of the proposed methodology is that it requires the bridge to be instrumented with inclinometers at many locations, which makes it economically.

1.3 Objectives

Given the shortcomings of available approaches in the literature and limitations in sensor technology, the main objective of his study is to develop a methodology of using the rotation response of a bridge to a moving load as a means of assessing its structural condition and to validate the approach experimentally at a laboratory scale. Numerical analyses are carried out to develop the theoretical basis of the proposed bridge damage detection methodology. Subsequently, a laboratory experiment is conducted on a 5.4 m long simply supported bridge structure to test the robustness of the proposed methodology. The test structure is instrumented with rotation sensors and axle detectors and a wide range of damage scenarios are investigated within the scope of this study. To give a context to this work, Section 2 explains the theoretical basis of the proposed bridge damage detection methodology and Section 3 explains the experimental study and describes the damage scenarios applied on the test structure. Section 4 presents the raw test data and elaborates on the preliminary processing. Finally, Section 5 presents the damage detection results from each test scenario investigated within the scope of this study.

2 Theoretical basis

This section presents the theoretical basis of the proposed bridge damage detection methodology. Numerical analyses are carried out on a 1-D bridge model to investigate the sensitivity of rotation as a main parameter to identify damage in a bridge. The hypothetical structure is modelled as a 17 m long simply supported bridge. The Elastic Modulus and Second Moment of Area assigned are 210 GPa and 12×10^9 mm^4, respectively. The hypothetical sensors (i.e. inclinometers / tiltmeters) are placed at four locations along the length of the bridge model, namely at the supports, at quarter-span and at three – quarter span locations. The bridge model is loaded with a 32-tonne moving point load. The numerical analyses carried out in this section develops the theoretical basis of the proposed damage detection methodology and demonstrates the concept. Therefore, the dynamics due to vehicle bridge interaction are not considered in the numerical analyses. Instead the load is applied statically and is moved incrementally across the length of the bridge model. Figure 1 shows the sketch of the bridge model, the sensor locations and the loading condition.
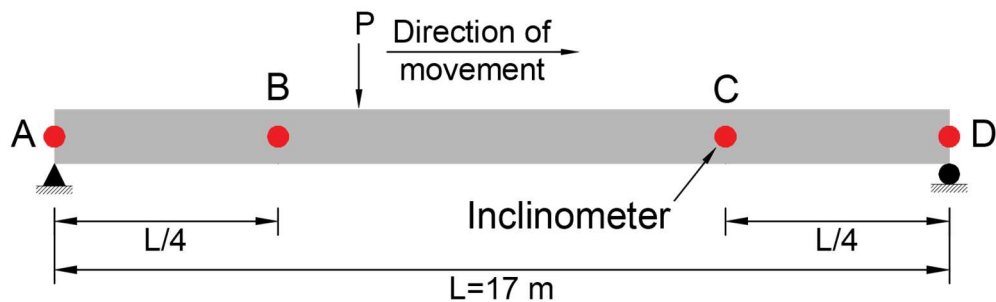

Figure 1. Sketch of the 1-D bridge numerical model

The effect of damage on the rotation responses of the bridge is investigated by simulating local damage at the bridge quarter-span location. The damage is modelled as a 15% reduction in stiffness over an 850 mm length (i.e. 5% of bridge span). The results from the simulation are presented in Figure 2(a). The solid blue curves in the figure show the rotation response of the bridge model obtained from Sensors A-D for the healthy bridge state whereas the dashed red curves represent the corresponding results for the damaged bridge state. In this study counter-clockwise rotation is taken as positive, therefore Sensors A and B experience negative rotations (i.e. clockwise) whereas Sensors C and D rotate in a positive (counter-clockwise) direction. It can be seen in the inset of the figure that when damage occurs, it results in an increase in rotation. The increase in rotation response due to damage is more evident for Sensor A than for other sensors. This is further investigated in the following analysis.

To further study the effect of damage, the differences between the healthy and damaged signals are identified by subtracting the damaged signals from the healthy ones, as presented in Figure 2(b). These rotation difference plots for all sensors are clearly triangular, and the maximum amplitudes in the plots for each sensor occur at quarter-span location, where the damage is simulated. The magnitude of the rotation difference plots, representing the sensitivity of a sensor to damage, is greatest for Sensor A with an amplitude of 2.5 millidegrees (mdeg). The corresponding results for Sensor B and Sensors C & D are 0.9 mdeg and 0.85 mdeg, respectively. Although Sensors C and D are at different locations, they have the same sensitivity to damage as the rotation difference plots overlay each other. The reasons for this are discussed further.
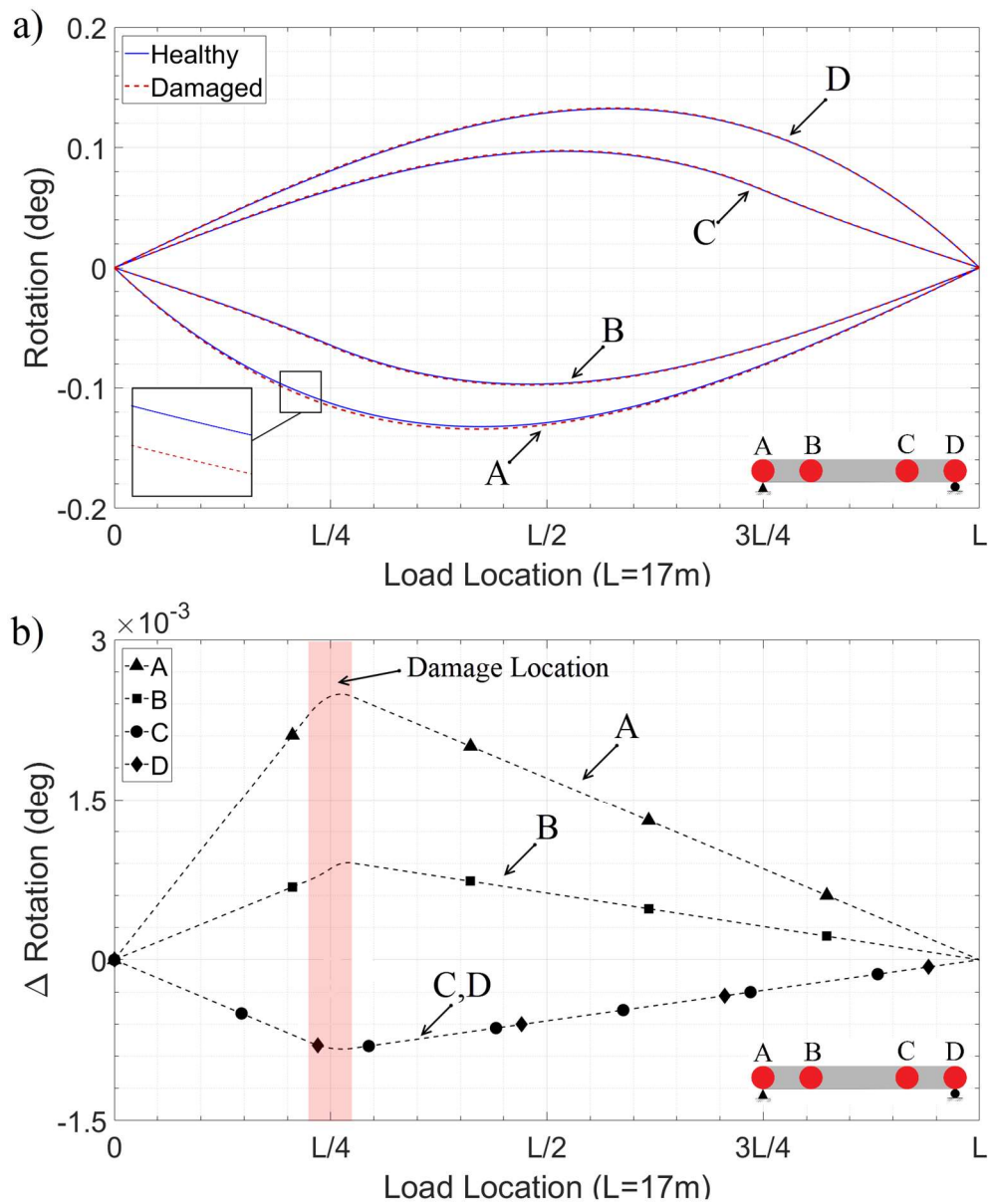
Figure 2 Effect of quarter-point damage on bridge rotation response to a moving single axle loading (a) Rotation time history recorded at Sensors A-D for healthy and damaged beam cases. (b) Corresponding differences between the healthy and damaged rotation signals shown in part (a).

11

Further analyses are carried to investigate how sensor location affects its sensitivity to damage. In the following analysis, the bridge model is loaded with a stationary point load placed at 3L/8. In this simulation with the stationary load, it is assumed that the bridge model is instrumented with an infinite number of sensors along its length. This allows the spatial variation in rotation measurements to be visualised, which in turn provides insight on the most suitable sensor location to identify damage in the bridge. The level and extent of damage investigated in this analysis are the same as the damage properties assigned in the simulation discussed above, i.e. the damage is modelled as a 15% reduction in stiffness over an 850mm length. Figure 3(a) shows a sketch of the bridge model, damage location and the loading condition.

Figure 3(b) plots the rotation at various points along the beam when the load is at 3L/8. The solid (blue) curve in the figure shows the rotation diagram for healthy bridge state whereas the dashed (red) curve corresponds to the results for damaged bridge state. It is shown in the figure (see insets) that damage (at quarter-span location) results in an increase in the magnitude of rotation measurements at various locations along the length of the beam. The increase in amplitude of rotation measurement is more evident (larger) on the left-hand side of the damage than for the opposite side of the damage. The reason for this is further studied in Figure 3(c) by plotting the difference in rotation between the healthy and damaged bridge states. It is showing that the rotation difference on either side of the damage is constant with a shift from negative to positive at the damage location. This simply demonstrates that a pair of sensors placed on one side of the damage have similar sensitivities, e.g., Sensors C & D coincide in Figure 2(b), and the sensor placed at the damage location fails to identify damage.

Another observation from Figure 3(b) is that the magnitude of rotation difference on the left-hand side of the damage location is 1.7 mdeg, which is greater than the corresponding results obtained on the right-hand side of the damage location (0.6

12

mdeg). This is because the damage is in the left-hand half of the bridge. Hence, sensors placed between the damage and the left-hand support are more sensitive to damage than sensors placed on the opposite side of the damage location.
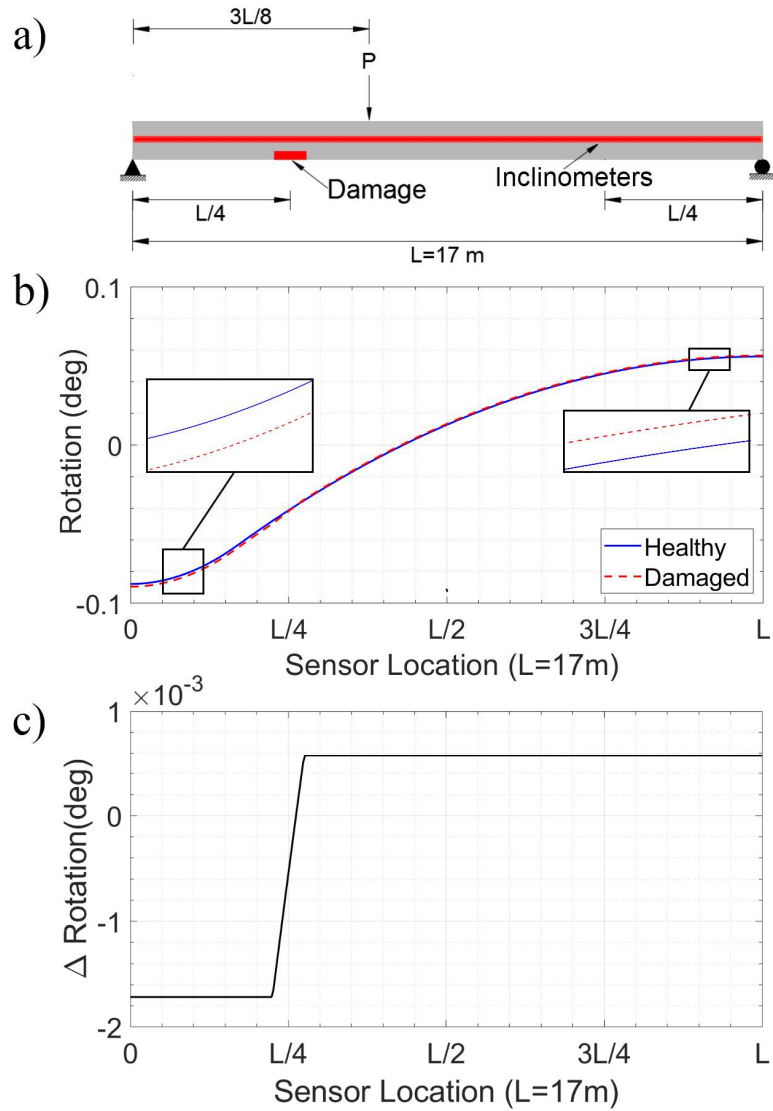

Figure 3. Rotation response of healthy and damaged beam models loaded with a single point load at 3L/8. (a) Sketch of the bridge model showing damage location, instrumentation and loading condition. (b) Rotation throughout bridge (c) Difference in rotation between healthy and damaged cases

13

Further analyses were carried out to identify suitable sensor locations for continuous bridges. This time the bridge is modelled as a two-span continuous beam element using the same structural properties describe above and loaded with a stationary point load placed at 3L/8 distance from the central pier location. The damage is simulated on the first span at L/4 distance from that support. The magnitude and extent of damage are modelled the same as that assigned in the previous simulation, i.e. 15% reduction in stiffness over an 850mm length. Figure 4(a) shows a sketch of the bridge model, damage location and the loading condition.

Figure 4 (b) shows the rotation diagram in the spatial domain for the healthy and damaged beam states. It is shown in the figure that (see insets) when damage occurs, the magnitudes of rotations at various locations along the length of the bridge increase, as expected. The differences in recorded rotations for the healthy and damaged states are presented in Figure 4 (c). It is shown in the figure that the magnitudes of rotation differences observed between the damage location and the closest support (i.e. pier location) are greater than the corresponding amplitudes obtained on the opposite side. This is because the damage is simulated closer to the right-hand support (i.e. at 3L/4 span location) on the first span. The sign of the rotation difference changes from negative to positive at the damage location. Unlike in a simply supported bridge, where the slope of the rotation difference was constant on either side of the damage, in a continuous bridge it is reducing from the damage location towards the support. It simply demonstrates that in a continuous span bridge, the most sensitive sensor location is in the vicinity of the damage location. However, while the largest amplitude of this signal occurs closer to the damage location, the rotation at the damage location is close to zero. Therefore, as the location of the damage in practice is not known a priori, placing the sensors at the supports is believed to be the most sensible option for continuous bridges as well.
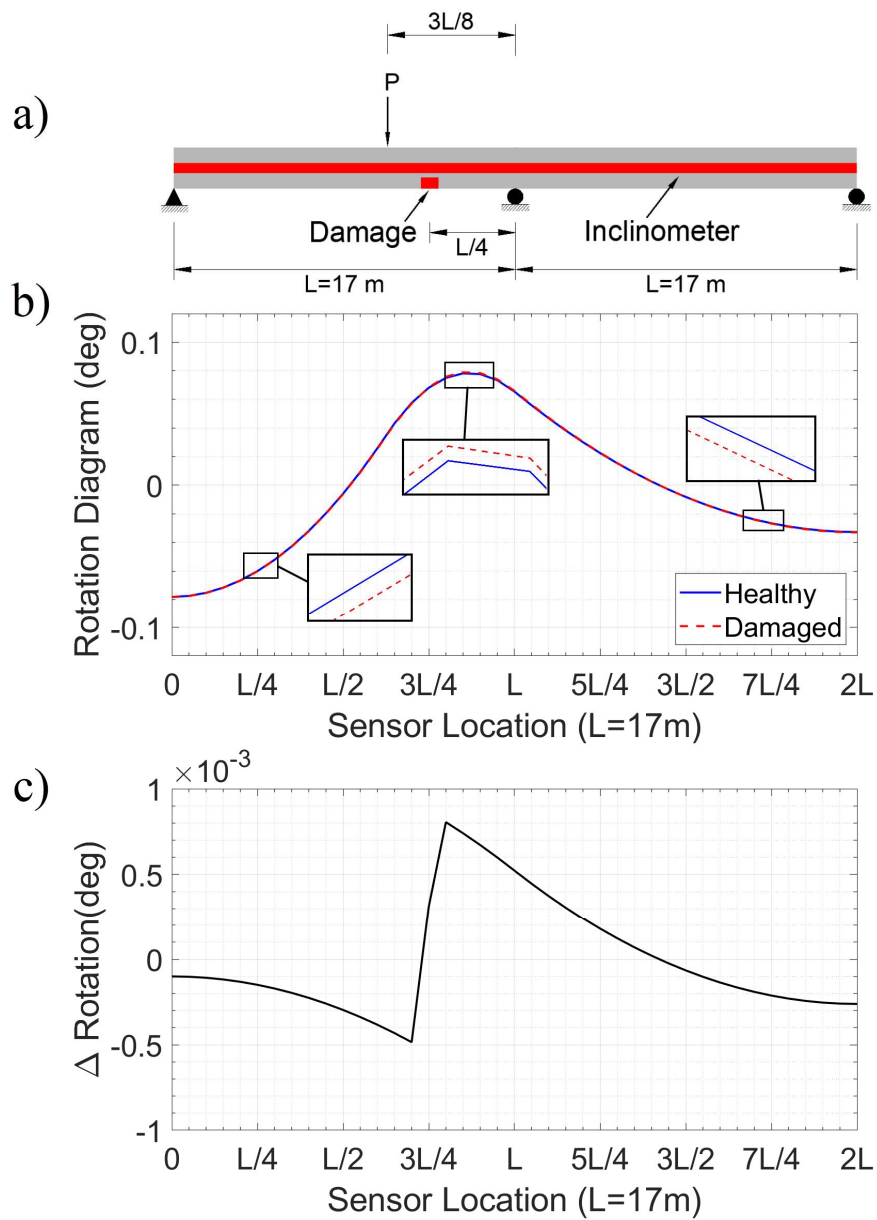
14

Figure 4. Rotation response of continuous healthy and damaged 2-span beam models loaded with a single point load at 3L/8 from the centre support. (a) Sketch of the continuous bridge model showing damage location, instrumentation and loading condition. (b) Rotation throughout bridge (c) Difference in rotation between healthy and damaged cases

From the analysis presented in Figures 3 and 4 it is concluded that supports are the most suitable sensor locations for rotation measurements. Since damage could occur at any location across the length of the structure, any sensor placed at the damage location could possibly fail to identify it. Besides, for simply supported bridges, the maximum magnitude of rotation occurs at support locations. Hence, sensors placed at supports are less affected by measurement noise. Installing the sensors at the ends of the deck also has practical advantages in the field as it is often easier to access the ends of the deck than it is to access areas toward the centre of the span.

The analyses carried out above demonstrate that rotation is a sensitive parameter to damage. Figure 2 shows that the rotation difference response to a moving point load for healthy and damaged bridge states identifies damage and its location. For multi-axle vehicles, the situation is more complex. A 32 tonne four-axle (moving) vehicle is now considered. Figure 5(a) is a sketch of the bridge model, hypothetical sensors, damage location and the loading condition. As before, damage is a 15% reduction in stiffness over 850mm length and is not considered.

The rotation signals obtained from the simulation are presented in Figure 5(b). For all sensors, there are slope discontinuities when an axle enters or leaves the bridge. Similar to the single axle moving load simulations, increase in the magnitude of rotation responses of the bridge is observed from all sensors due to damage.

In this case, the rotation difference plots (Figure 5(c)) are not exactly triangular and the peaks are not at the damage locations, making it difficult to identify damage. This is because each plot in Figure 5(c) is in effect the sum of triangles for each individual axle. This is further illustrated in Figure 6 where the breakdown of plots for Sensor A are presented.
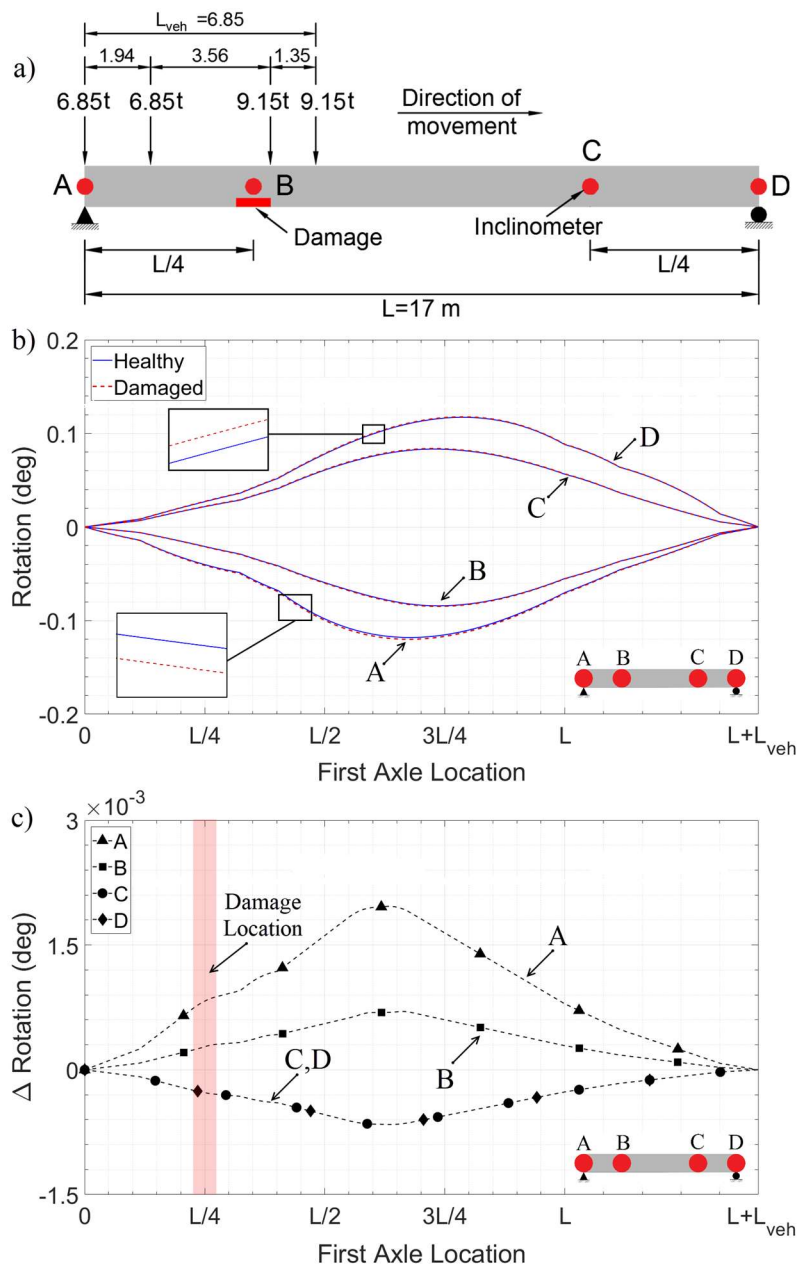
Figure 5. Effect of quarter-span damage on bridge rotation response to a moving multi-axle vehicle (a) Sketch of the bridge model showing damage location, instrumentation and loading condition. (b) Rotation response recorded at Sensors A-D for healthy and damaged bridge cases. (c) Difference in rotation measurements between healthy and damaged states
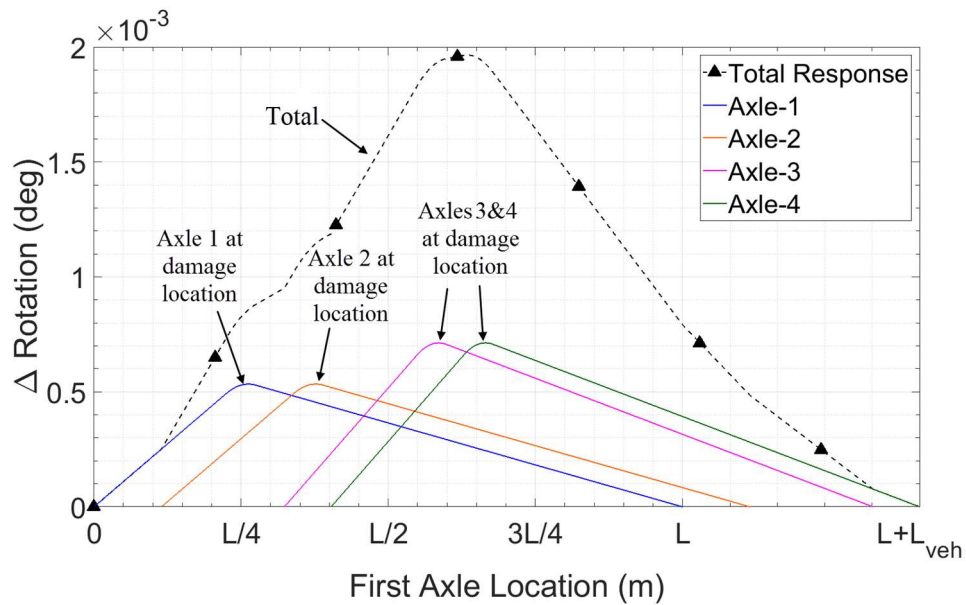
Figure 6. Difference in rotation measurements at A and contributions to the difference from each axle.

Using Bridge Weigh-in-Motion theory, it is possible to back calculate the rotation unit influence line (IL) of the bridge from its response to the vehicle of known weight and axle configuration. Since IL is a unique structural property and represents the response of a bridge to a unit load, the rotation IL difference for healthy and damaged bridge states should identify damage and its location. Obtaining the IL is possible [53–56], providing that the traversing vehicle axle weights and spacings are known, which would be the case if a Weigh-In-Motion system were present.

In this study, rotation ILs are calculated from the responses of Figure 5 using the process proposed by O'Brien et al [55] at are shown in Figure 7 (a). As for responses to single-axle moving loads, the rotation IL difference plots for all sensors, shown in Figure 7 (b), are triangular with a peak at the damage location.

18

In a previous study [57], the authors tested the robustness of the proposed damage detection methodology in a series of blind tests. A 3-D dynamic Finite Element model of a 20 m long simply supported bridge structure, developed and run by an independent team of researchers, was used as the reference data. Rotations from an extensive range of damage scenarios were provided to authors by the independent team who applied the damage detection methodology without prior knowledge of the extent or location of damage. Results from the blind tests demonstrated that the proposed methodology provides a reasonable indication of bridge condition for all the simulated test scenarios. In the following section, the proposed methodology is tested through an extensive laboratory experimentation conducted on a 5.4 m long simply supported model bridge.
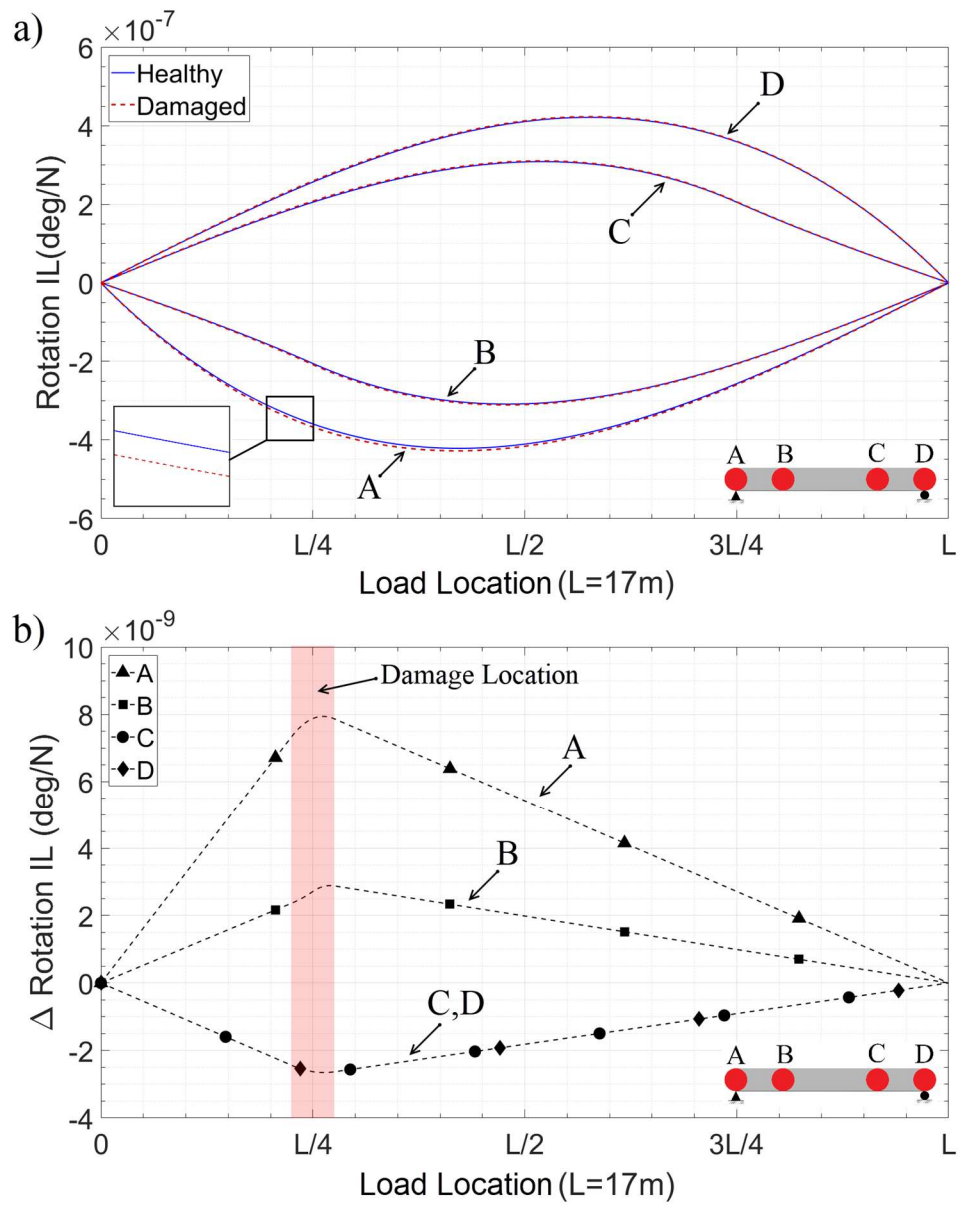
Figure 7. Effect of damage on calculated rotation influence lines (a) Rotation influence lines (b) Difference in rotation influence lines between healthy and damaged states

3   Laboratory Experiment

An experimental study is carried out on a 5.4 m long simply supported bridge in the laboratory to validate the results obtained in the previous section. The test structure is instrumented with rotation sensors and axle detectors and loaded with a four-axle moving vehicle. In this study, rotations are recorded using high grade force balance Damage scenarios are investigated by locally changing the stiffness of the bridge. Instead of damaging the bridge, it is stiffened using steel plates bolted on to the flanges, effectively applying "negative damage". An advantage of this approach is that it allows the test structure to be reused after each test case and to investigate a wide range of damage scenarios. Section 2.1 describes the test layout and instrumentation and Section 2.2 describes stiffening application and the test scenarios investigated within the scope of this study.

3.1   Test layout and instrumentation

The test structure is a simply supported bridge made of a 5.6 m long steel I-section oriented in the weak direction (i.e. web is horizontal). The Modulus of Elasticity and Second Moment of Area obtained from the supplier are 210 GPa and 11.6×10^{-7} m^4, respectively. The boundary conditions of the model are designed as a pin-roller support. It is 300 mm wide and the distance between supports is 5.4 m. Figure 8 (a)-(c) shows the elevation, cross-sectional dimensions, and the roller support, respectively.
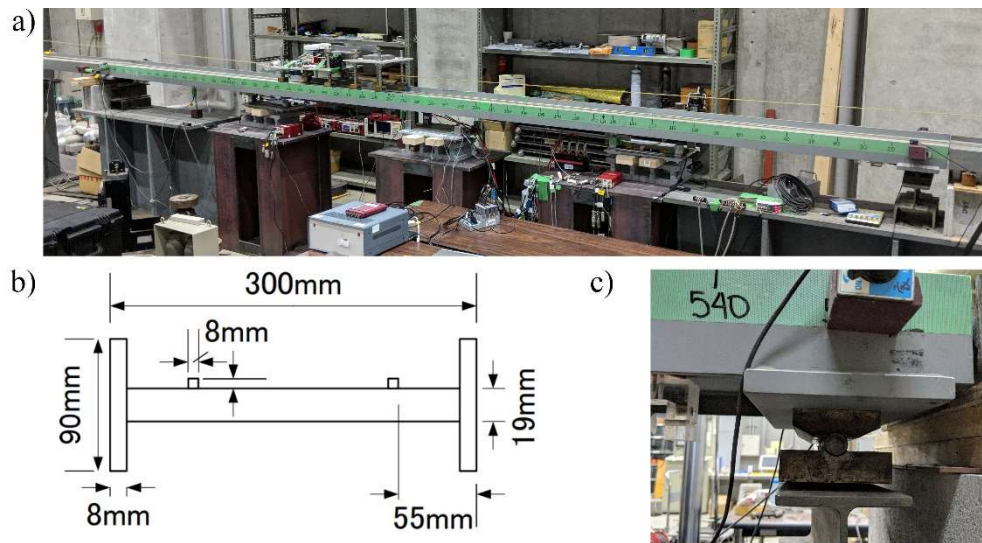
Figure 8. Test structure (a) Elevation (b) Cross-sectional dimensions (c) Roller support

The bridge also incorporates 8 mm square steel rails on which the wheels travel. The rail is designed to have a 'very good' (Class A) road surface profile according to ISO [58]. The vehicle itself is a four-axle tractor-trailer, propelled by a motor and pulley system. Its speed is maintained by a constant electronic controller as it crosses the bridge. Approach spans are provided at the entrance and exit to allow for acceleration and deceleration. Once the vehicle enters the bridge it travels with a constant speed of 1.05 m/s. The axle weights of the vehicle were determined using a weighing scale with a precision of ±100 grams. Figure 9 shows the vehicle model on the bridge at the midspan location and Table 1 gives its axle weights and spacings.
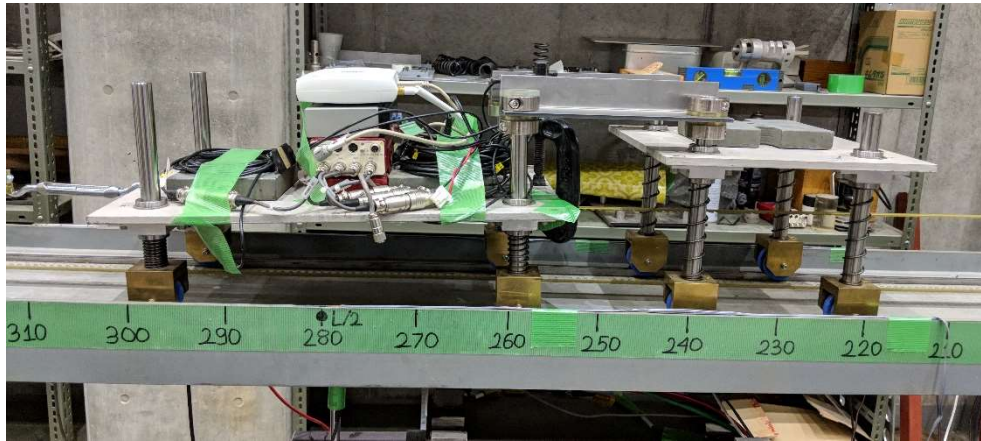
Figure 9. Model Vehicle

Table 2. Vehicle model axle configuration

Axle Number	Weight (kg)	Axle spacing (mm)
Axle 1	12.7	0
Axle 2	14.75	400
Axle 3	8.05	210
Axle 4	6.7	190

The structure was instrumented with accelerometers and laser axle detectors. Laser axle detectors were placed at the start and end of the bridge to identify the entrance/exit of an axle. The data from the axle detection system was later used to calculate the speed and the axle spacing of the vehicle. In this study, rotations were recorded using Honeywell QA-750 sensor accelerometers placed in the bridge longitudinal direction at the two supports, quarter and three-quarter span locations. Data acquisition was carried out at a 512 Hz sampling rate using an NI9234 data acquisition system controlled by a computer. Figure 10 shows the sensor locations, a Honeywell QA-750 accelerometer and one of the laser axle detectors.
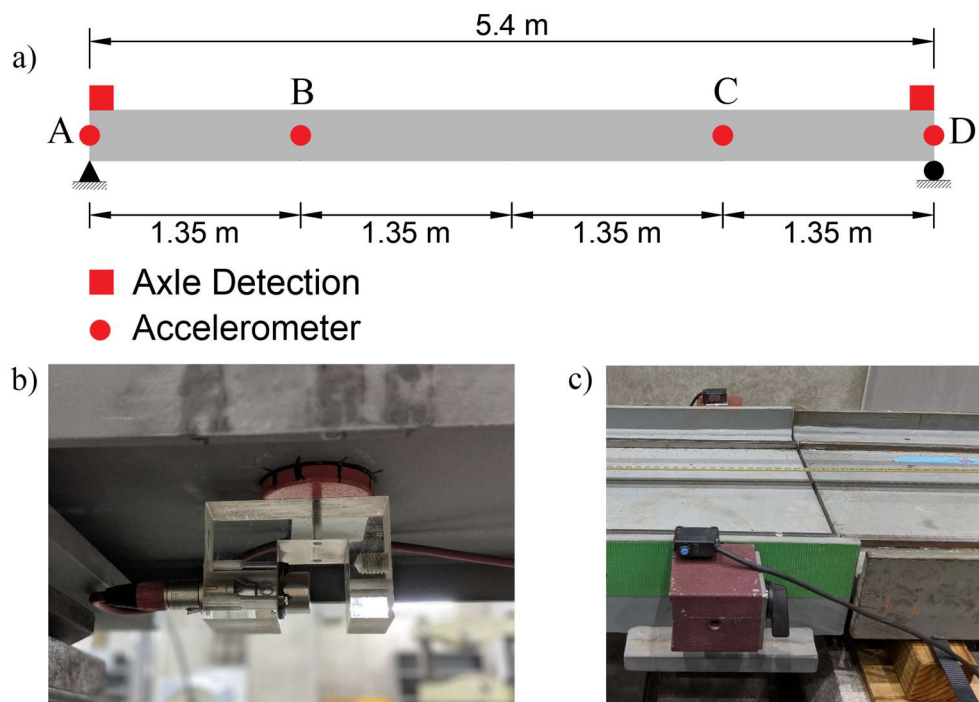
Figure 10 Test layout and instrumentation (a) Sketch of the bridge showing sensors and their locations (b) Accelerometer sensor at point A (c) Axle detection sensor at point A

Recent works examined the relevant attributes of Honeywell QA-750 accelerometer for SHM applications [59, 60]. One of the capabilities is that these accelerometers can sense frequencies as low as 0 Hz, so they can sense gravity and are suitable for use as inclinometers. Another finding from these studies is a very low noise level. In another study conducted on a railway bridge [61], authors measured rotations at five locations along the length of a bridge and using this and the available methodology in literature [48], calculated the midspan deflections of the bridge deck. Calculated midspan deflections were later validated with deflections measured with an optical camera system.

3.2   Stiffening application and test scenarios

The structure was loaded with the moving four-axle vehicle to obtain reference data for its healthy state. The vehicle crossed the bridge 12 times at a speed of 1.05 m/s, which is the maximum allowable speed at the test facility. Then, the structure was stiffened locally by clamping steel plates to the sides of the flange using stiffening bars and steel bolts as shown in Figure 11 (a). Stiffening bars were fabricated with the same thickness as the bridge flanges and were placed between the stiffening plates. The stiffening plates were then attached to the bridge by tightening M10 bolts at their ultimate torque capacity. The aim was to clamp the stiffening plates to the bridge as tight as possible to provide good shear transfer. Figure 11 (b) shows the plates attached to the test structure

The stiffening plates were fabricated in various cross sections and lengths to study a range of damage scenarios.

- The plates were designed to increase the Second Moment of Area of the bridge by 50%, 25% and 16%. For those test scenarios aiming to increase the Second Moment of Area by 50% the stiffening plates were attached on both sides of the bridge (see Figures 11 (c) and (d), whereas for the test cases with 25% and 16% increase in stiffness the plates were attached on one side only.

- The lengths of the plates were fabricated as 400 mm, 270 mm and 135 mm, corresponding to 7.5%, 5% and 2.5% of the bridge span, respectively. Figures 11 (c) and (d) show the longest and shortest plates, attached at midspan.

- The stiffening plates were attached to the bridge at three different locations, one at a time, namely, midspan, quarter-span and three-quarter span.
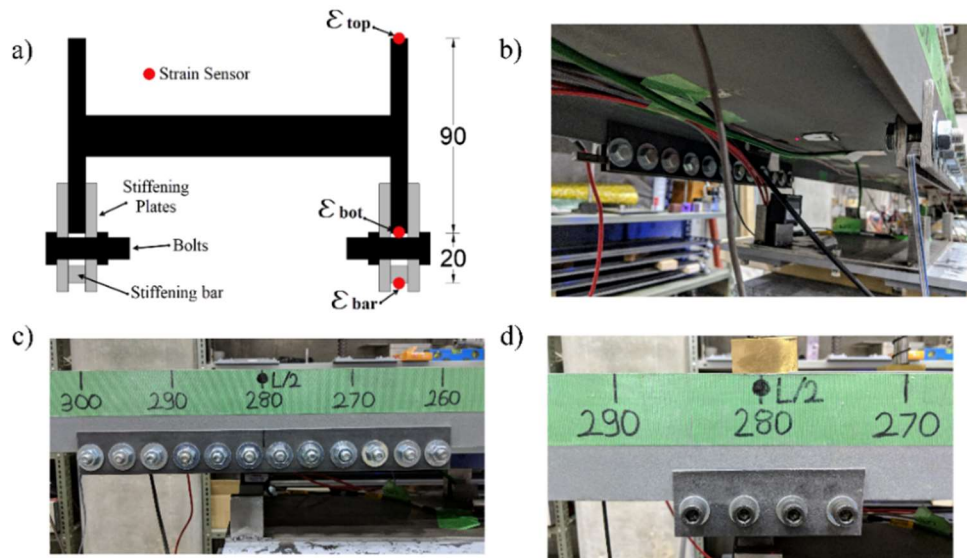
Figure 11. Local stiffening of bridge (a) Cross-section (b) Side view of stiffening plates attached to the bridge (c) Elevation of 400 mm long (7.5% of span) stiffening plates attached at midspan (d) Elevation of 135 mm long (2.5% of span) plates at midspan

The level of shear transfer between the stiffening plates and the bridge depends on the magnitude of the torque applied to the bolts as well as the plate length. From a basic assumption of elastic beam theory, providing full shear transfer is achieved, plane sections should remain plane. In other words, the slope of the strain diagram through the depth of the cross section should be constant. To check if this was true and to identify the effective level of stiffening that was actually achieved, strain sensors were installed at the stiffening locations and the level of shear transfer was calculated for each stiffening application by investigating the cross-sectional strain diagram of the bridge. The strain sensors are placed at the top and bottom of the flanges (ε_{top} and ε_{bot}) and at the bottom of the stiffening bars (ε_{bar}) at the centreline of the stiffening location, as shown in Figure 11 (a). It was found that the level of shear transfer was governed by the length of stiffening plate used and this was true, no matter where along the length of the bridge, the stiffening was applied. Figures 12 (a), (b) and (c) present the results for 400

mm, 270 mm and 135 mm long plates, respectively. In each case, the raw strain data histories are given under arbitrary static loading and the equilibrium values of strain at the top, bottom and stiffening bar levels.

It can be seen in Figure 12 (b) that strain varies linearly with respect to cross section depth for the 7.5%L stiffener. This confirms the assumption of plane section remaining plane under bending and it can be inferred that full shear transfer is achieved.

A slope discontinuity is evident in Figure 12 (b) implying that full shear transfer has not occurred between stiffening plates and the bridge. In other words, the bridge is only partially stiffened. To quantify the effective level of stiffening, the strain diagram was extrapolated (dashed blue line) and the resulting strain compared to the corresponding measured value, ε_{bot}. The ratio of measured (28.6) to expected strain (34.8) at the bottom of the stiffening bar is referred to as the peak stress ratio,82% in this case. The level of shear transfer is calculated similarly for the 2.5% L plates. In this case the peak stress ratio is found to be 44%. It should be noted that the strain diagrams across the cross section of the bridge are obtained at the centreline of the stiffening point. The strain distribution along the length of the stiffener is likely to be different hence the stress ratio is only a rough indication of the effective stiffness increase.
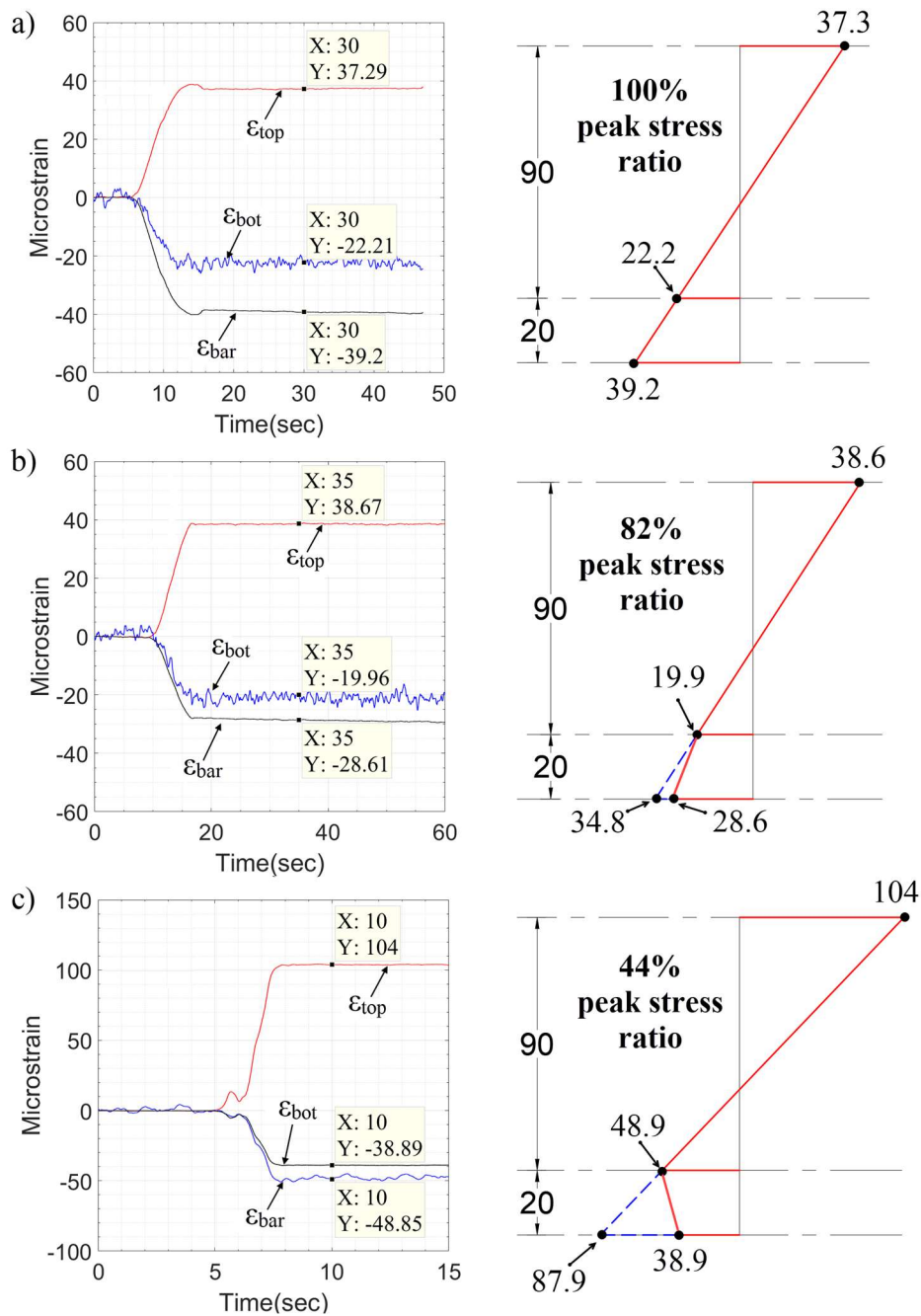
Figure 12. Measured strain histories and calculated peak stress ratio for (a) 7.5%L (400 mm) long plates, (b) 5%L (270 mm) long plates and (c) for 2.5%L (135 mm) long plates

In this study, a wide range of test scenarios are investigated which include single and multiple stiffening cases. For single stiffening test cases, the bridge was stiffened at three different locations, one at a time, across the length of the structure, namely at

28

midspan, quarter-span and at 0.85L, where L is the bridge span. In total nine single-stiffening test cases were investigated at each location, made up of the combinations of three different cross sections and three different lengths of stiffening plate. Table 3 tabulates the single stiffening test cases investigated at each stiffening location. An 'effective stiffening factor' is used here as an indication of the level of stiffening achieved. It is defined as the product of the target increase in second moment of area and the peak stress ratio. A 100% peak stress ratio clearly indicates that the target increase in stiffness has been achieved and lesser peak stress ratios imply some level less than the target. Two multiple stiffening test cases were investigated as listed in Table 4. In the first, short plates are attached at quarter-span and 0.85L. In the second case, the first short plates are moved to mid-span.

Table 3. Effective stiffening factor for single stiffening test cases applied at three different locations (i.e. L/4, L/2 and 0.85L).

Plate length, L_{plate} (in mm)	Peak stress ratio	Target increase in second moment of area		
		50%	25%	16%
400	100%	50%	25%	16%
270	82%	41%	21%	13%
135	44%	22%	11%	7%

Table 4. Multiple stiffening test cases

Test Case	1st Stiffening			2nd Stiffening		
	Location	Extent	Effective Stiffening factor	Location	Extent	Effective Stiffening factor
M1	L/4	270 mm	21%	0.85L	270 mm	21%
M2	L/2	270 mm	13%	0.85L	270 mm	41%

4 Raw test data and preliminary processing

Figure 13 presents typical raw data from the axle detection system for one vehicle pass. Spikes in the voltage can be seen for the entry times (red solid) and exit times (the dashed) of each axle in the 4-axle vehicle. The average speed of the vehicle is calculated from the average time difference and the known length between sensors. The vehicle speed is maintained by a constant electronic controller and the vehicle is assumed to be travelling at a constant speed while it is on the bridge.
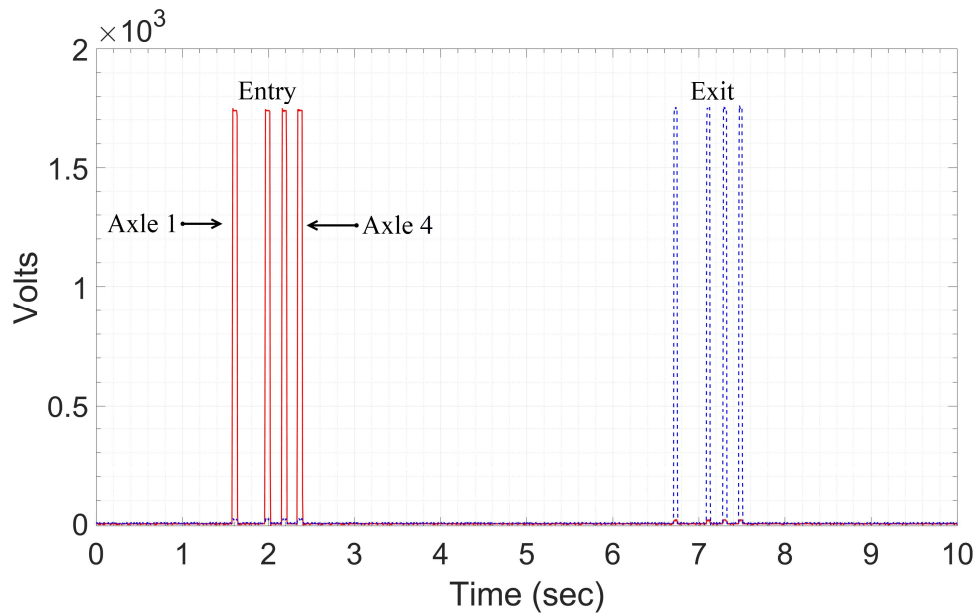

Figure 13. Results obtained from axle detection system

The output from each of the four accelerometers follows a sinusoidal relationship when it is rotated through gravity, i.e. when it is positioned vertically up, horizontally and vertically down, it reads 1g, 0 and -1g, respectively. From basic trigonometry, rotations were calculated by applying the inverse sine function to the acceleration data.

The underlying assumption when calculating rotation measurements from accelerometers is that the only acceleration response is that associated with rotation

31

through gravity. However, in practice, as well as experiencing rotation due to the static effects of the load on the bridge will also contain a low level dynamic response and noise. Figure 14 (a) shows the raw acceleration time history obtained from Sensor A for one vehicle pass. The excitation that occurs in advance of the vehicle entering the bridge and after leaving the structure represent the measurements captured by the sensor while the vehicle is travelling on the acceleration/deceleration spans. It can be seen in the figure that the acceleration response has a roughly parabolic shape (static part) with considerable high frequency content (dynamic part). A low pass filter is applied on the raw acceleration data with a cutoff frequency of 0.5 Hz to remove the high frequency content of the response. Subsequently, the rotation values are obtained by taking the inverse sine function of the filtered data. Figure 14(b) shows the corresponding calculated rotation signals for Sensors A-D. The maximum amplitude of rotation measurements is approximately 0.18 degrees.
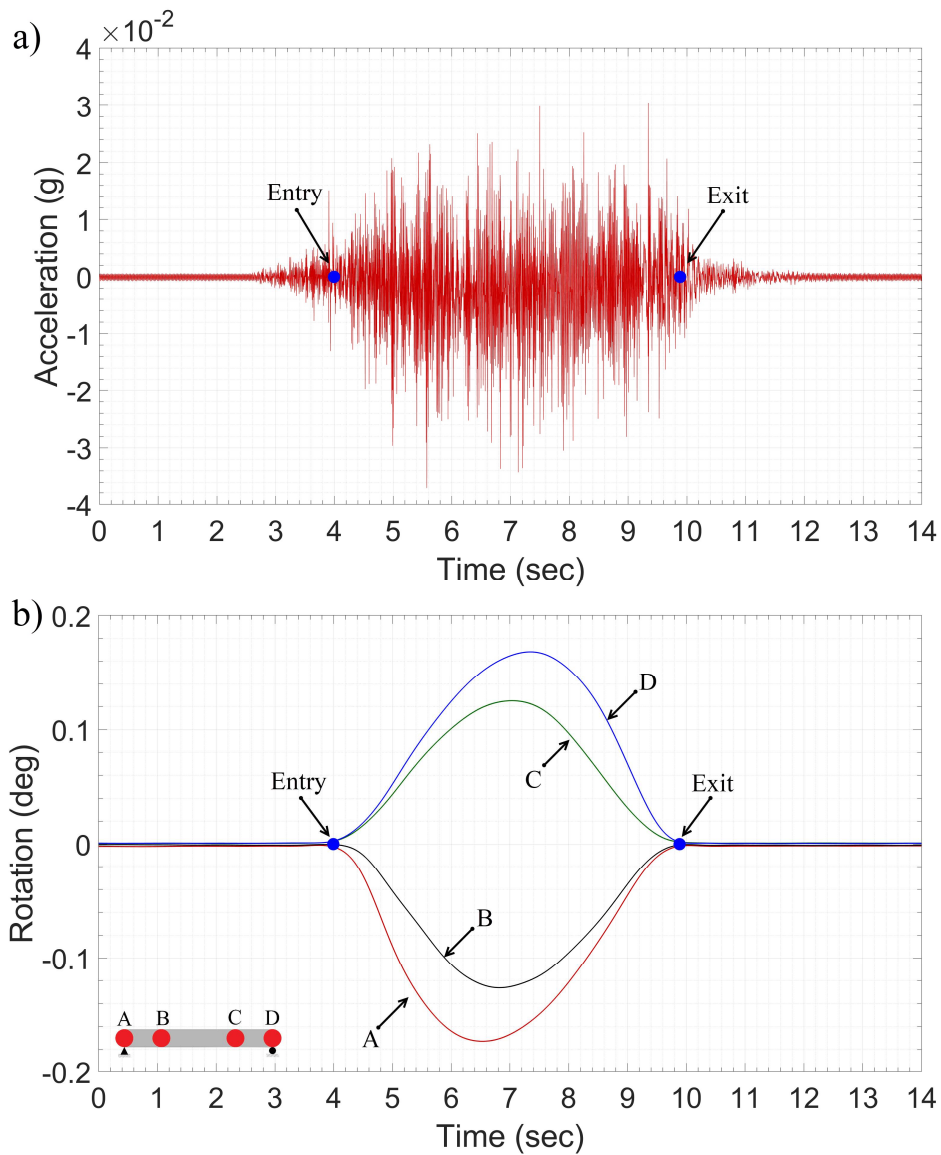
Figure 14. Effect of vehicle crossing bridge (a) Acceleration time history of Sensor A (left support) (b) Rotation time histories calculated from measured accelerations

Laboratory experimentation, in particular the weight of the vehicle model, were designed such that the magnitudes of measured rotations on the bridge model would represent the magnitudes of measurements expected in a real bridge. Figure 15 presents the rotation response of a 17.8 m long bascule bridge, recorded using the same accelerometers, during the passage of a 32 tonne four-axle truck. When the bridge is

down, it behaves as if simply supported. The maximum amplitude of rotations obtained from the test structure is approximately 0.12 degree, i.e. a similar order of magnitude to that recorded in the laboratory tests.
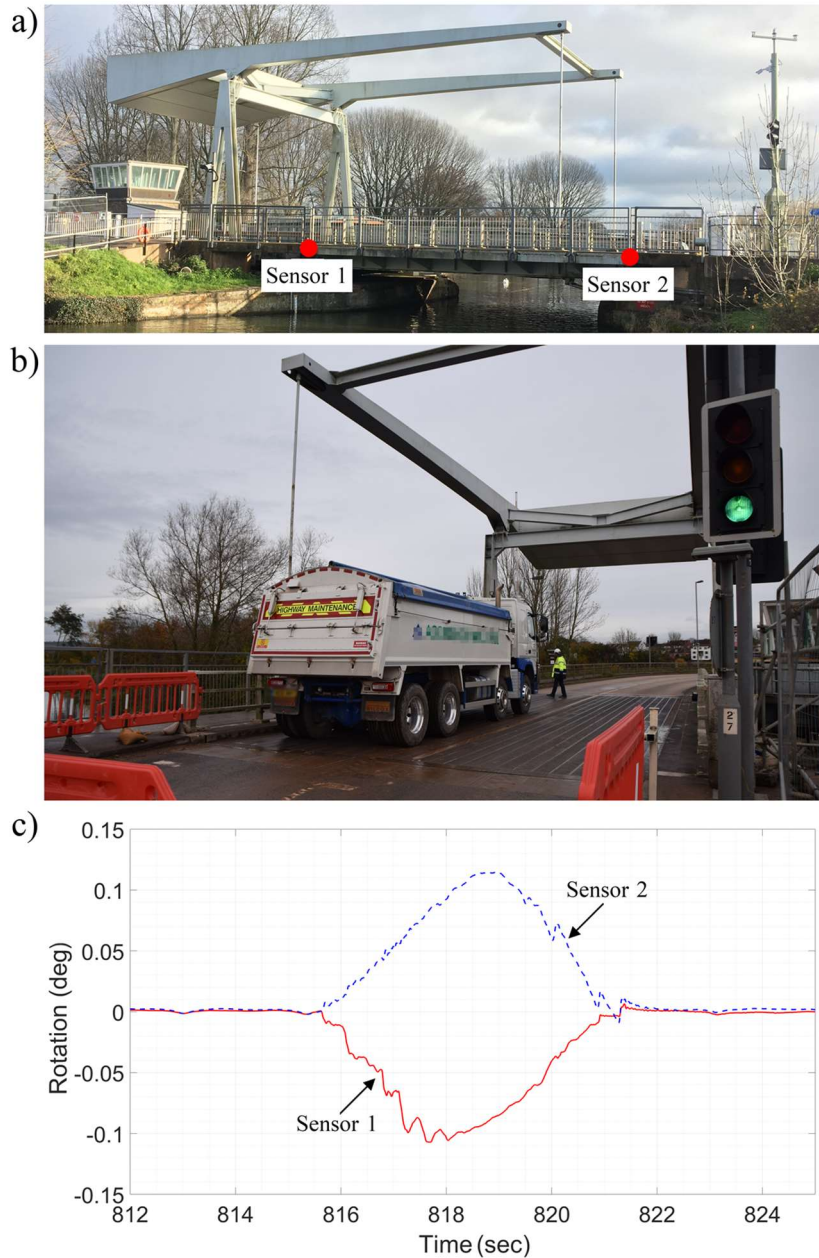

Figure 15. Rotation measurements on a real bridge (a) Test structure (b) Four-axle 32 tonne test truck (c) Rotation time history recorded at supports

The rotation ILs of the laboratory bridge model are calculated using the procedure described by OBrien et al [55]. The procedure uses the rotation responses of the bridge (Figure 14 (b)) to a vehicle of known speed and axle configuration to calculate the rotation ILs. Figure 16 presents the rotation ILs calculated from the Sensors A-D signals for the healthy bridge state. The vehicle crossed 12 times and the IL for each sensor was calculated for each pass of the vehicle. The inset in the figure shows a zoomed view in the figure and it can be seen that there is good repeatability in the IL calculations proving the reliability of the methodology used in this study for obtaining ILs.
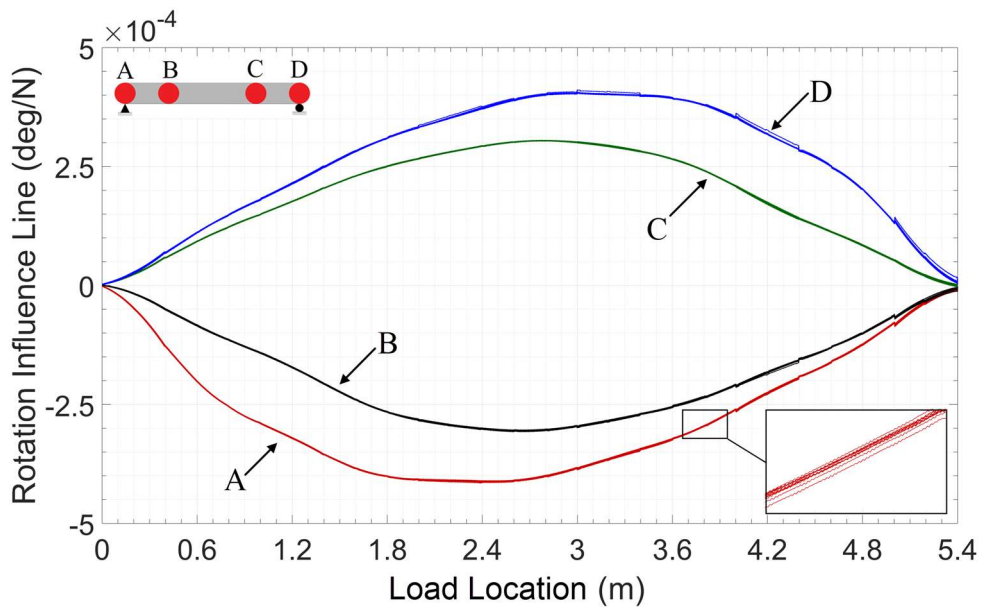

Figure 16. Calculated rotation influence lines for Sensors A-D based on twelve vehicle runs on the healthy bridge

5   Damage Detection results

The average of the rotation ILs obtained for each damaged bridge state is subtracted from the corresponding average rotation IL for the health bridge state. Figure 17 presents the resulting rotation IL differences for the nine test cases tabulated in Table 3 for midspan stiffening. Each chart in the figure shows the results for sensor locations A, B, C and D indicated by red, black, green and blue plots, respectively (see legend by). It can be seen that for all nine test cases, the shapes of the rotation IL difference plots are approximately triangular and the maximum amplitudes occur at the midspan location where the stiffening plates were attached. Moreover, the amplitude of the plots is approximately proportional to the effective stiffening factor, (y axis limits for rows 1, 2 and 3 of the figure are ± 6, ± 4.5 and ± 1.5 x 10^{-7} deg/N, respectively). These plots demonstrate that, when the stiffening is applied at midspan, the proposed methodology can successfully identify stiffening application as low as 7% change in Second Moment of Area over 130 mm (2.5% bridge span). For this damage location, the sensor location has little effect as the maximum amplitude of rotation IL difference plots is roughly the same for all four sensors.
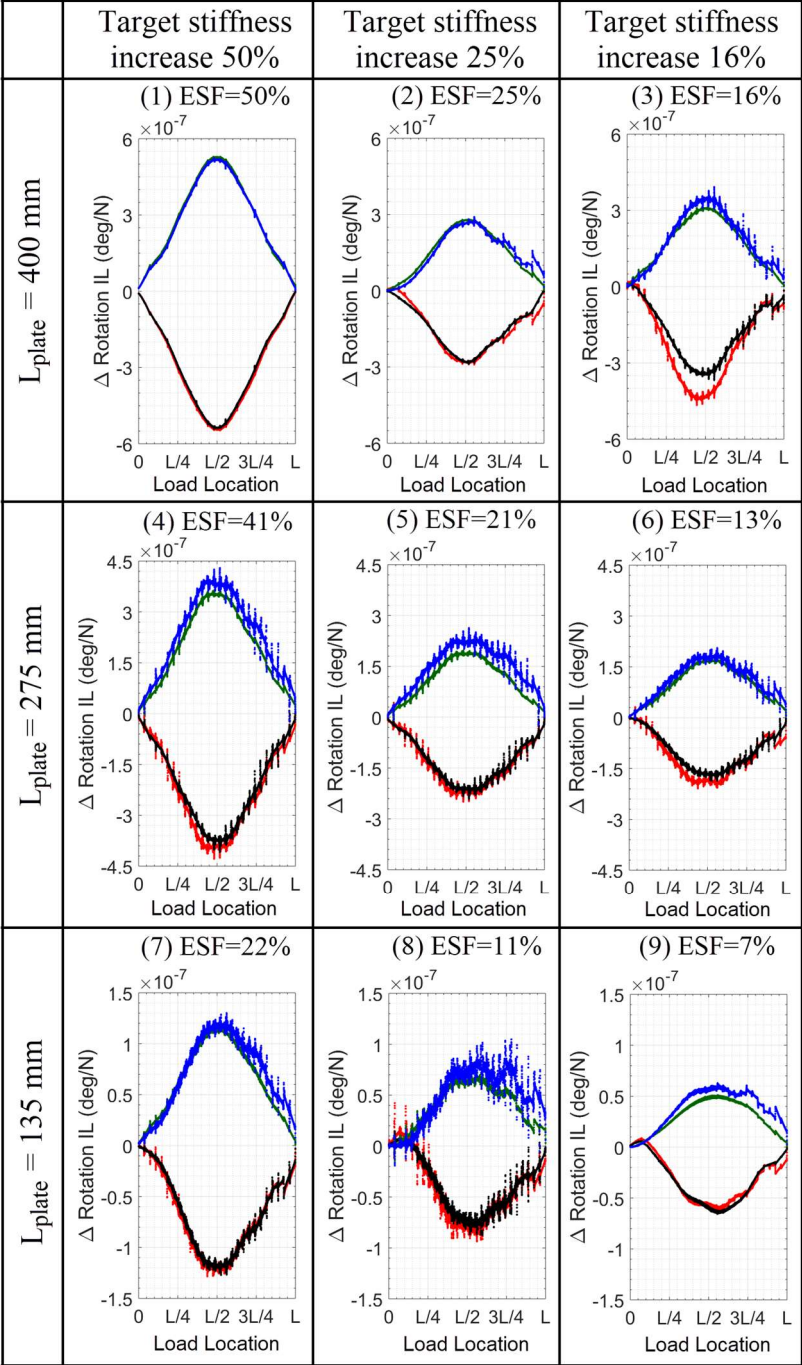
Figure 17. Difference in rotation influence line plots for stiffening applications at midspan. ESF = Effective Stiffening Factor

The corresponding results for the nine test scenarios (Table 3) when stiffening is applied at the quarter-span location, are presented in Figure 18. In this case, some sensors are clearly more sensitive than others. As discussed previously (Figures 2 and 3) for a simply supported bridge:

(i)   sensors on the same side as the damage experience approximately the same change in rotation,

(ii)   the greatest change in rotation occurs in the zone between the damage and the support nearest to it and

(iii)   sensors at, or very close to the damage location are not particularly sensitive to damage.

Hence for damage at the quarter-span, sensor A has the greatest amplitude with the other three sensors having approximately similar, lower, amplitudes. For this sensor, the results are reasonably good for all cases and the response is roughly triangular with a peak close to the damage location. Sensors B-D fail to detect the stiffening for those cases where the effective stiffening factor is smallest.
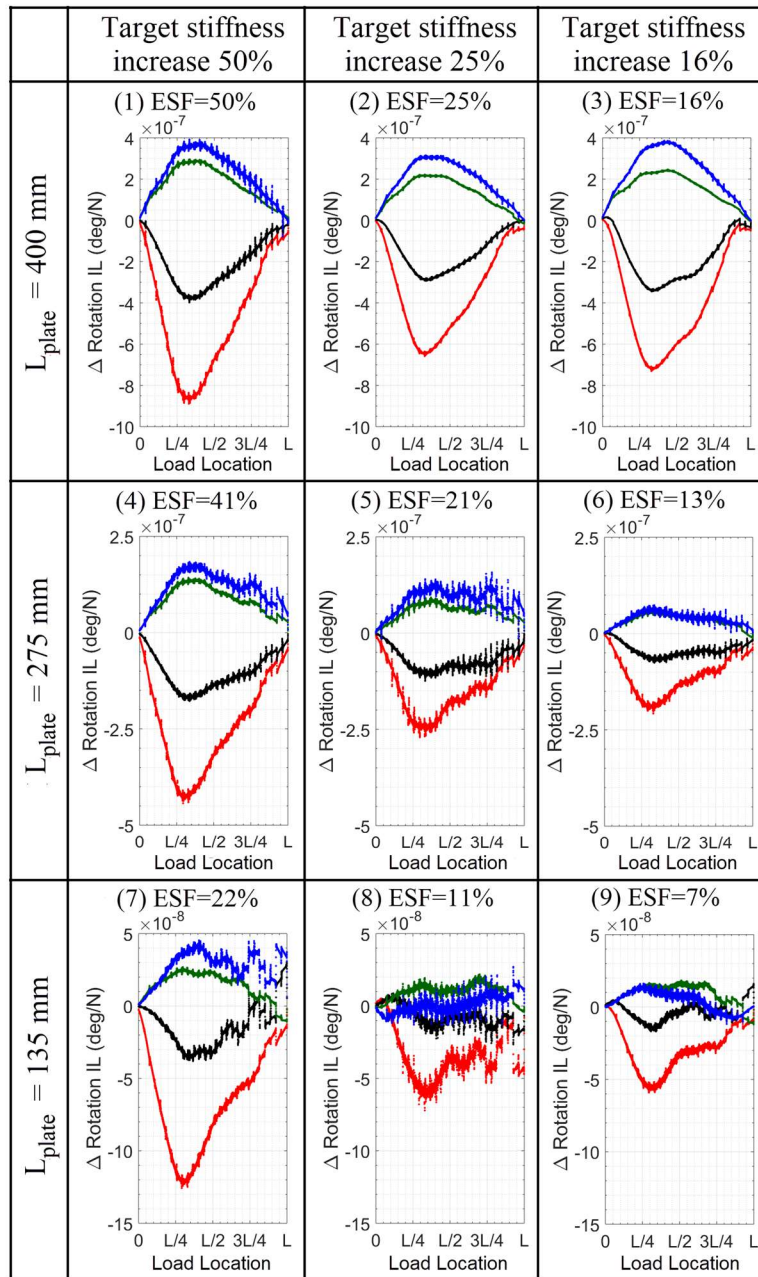
Figure 18. Difference in rotation influence line plots for stiffening applications at quarter-span. ESF = Effective Stiffening Factor

The amplitudes of the plots presented in Figure 18 are approximately proportional to the effective stiffening factor. This is illustrated in Figure 19 by plotting the maximum

amplitude of rotation influence line differences obtained from all sensors for nine stiffening test scenarios applied at the L/4 span location. The top three figures in Figure 19 are just reproductions of the first three test scenarios presented in Figure 19 and are included here to show where the data in the figure is coming from. For each damage scenario with the same length of stiffening plates (Test scenario Nos. 1 – 9) the maximum amplitude of rotation influence line generally reduces as the ESF reduces, as expected. It can be seen that this is not universally true when the 400 mm plate with 25% ESF is applied on the bridge as the maximum amplitude of rotation IL differences is lower than the corresponding results for 16% ESF with the same length of plates. The reason for this may be slippage between the stiffening plates and the bridge. Overall, these plots demonstrate that the magnitude of ESF and the length of the plates, which defines how much the bridge is stiffened, is strongly correlated with the maximum amplitude of rotation IL difference.
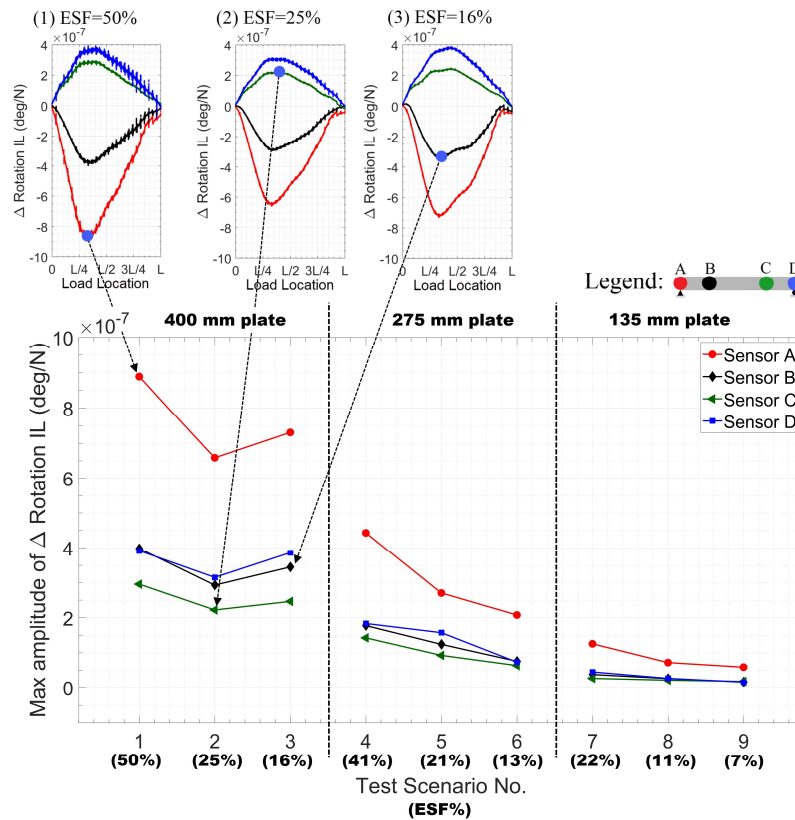
Figure 19. Maximum amplitudes of rotation influence line plots as a function of ESF for stiffening at L/4.

The damage detection results when the stiffening plates are located at 0.85L are presented in Figure 20. The results for test case Nos. 1-2 and from Sensor-C in test case No. 7 are not presented due to corrupted data. It can be seen that the shape of the rotation IL difference plots from Sensor D, which is at the support nearest the damage, is triangular for all the test scenarios. The peaks in the plots occur at around the three-quarter span location, offset from the stiffening location (i.e. 0.85L). From the corresponding results at Sensors A-C, it is not possible to identify damage as the shape of the rotation IL difference plots are not triangular. The sensitivity of these sensors is low as they are in the zone between the damage and the support furthest from the damage.

41

Overall, Figures 17, 18 and 20 show that the proposed bridge condition monitoring methodology can successfully identify cases of single stiffening in the model bridge. For the stiffening applications carried out off centre (Figures 18 and 20), only the sensor in the zone between the damage and the support closest it, identified the presence of stiffening for all nine test cases. The other sensors identified the damage location only for higher strengthening levels.

In Figure 18 (strengthening at 0.25L) Sensor A identified the stiffened bridge states for all test cases and in Figure 20 (stiffening at 0.85L) Sensor D identified all damage locations. This suggests that, providing a bridge is instrumented with rotation sensors at both supports, the proposed bridge condition monitoring methodology can successfully identify damage at any location across its length.
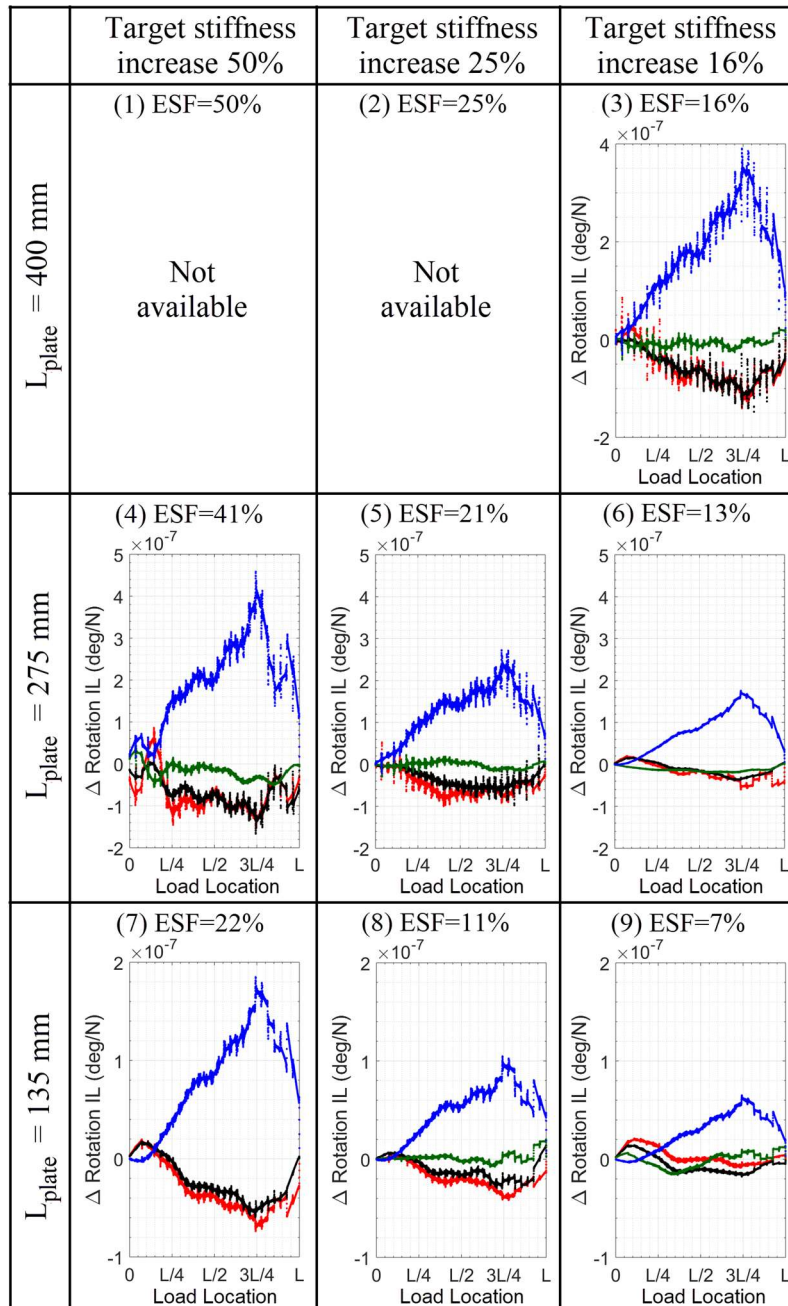
Legend: A B C D

Figure 20. Difference in rotation influence line plots for stiffening at 0.85L. ESF = Effective Stiffening Factor

43

Figure 21(a) presents the results for multiple stiffening test case No.1, as detailed in Table 4. In this case, stiffening plates are attached at two location across the length of the bridge, at quarter-span and at 0.85L. It can be seen in Figure 21(a) that the rotation IL difference plots obtained from Sensors A and D are roughly triangular, suggesting the presence of stiffening. The maximum amplitude in the plot for Sensor A is slightly offset from the quarter-span location, where the nearer stiffening plates were attached. For Sensor D the maximum amplitude of the rotation IL difference plot is at the three quarter-span location, again offset from the nearer stiffening plates. For Sensors B-C, there are no apparent triangular shapes in the plot and they fail to identify the presence of stiffening. The results obtained from Figure 21(a) agree well with those for the single stiffening test scenarios. In essence, sensors in the zone between the damage and the support nearest damage (i.e. Sensor A and Sensor D in Figure 21(a)) identified the stiffening and sensors in the zone between the damage and the support furthest from it (Sensors B-C in Figure 19(a), fail to identify the damage.

The damage detection results from multiple stiffening test case No. 2 are presented in Figure 21(b). In this case, stiffening plates were attached at midspan and 0.85L and the Effective Stiffening Factor were 13% and 41%, respectively. It can be seen in the figure that the maximum amplitudes of rotation IL difference plots from Sensor A-C are around the midspan location where the smaller plate stiffener is located. The Sensor D results have a peak at the three-quarter span location, slightly offset from the location of the larger plate stiffener. Thus, as before, both damage locations can be identified, with different sensors sensitive to each. It is interesting that Sensor D does not identify stiffening at the midspan location as its effect is less than that of the larger plates at 0.85L. This also demonstrates that, if multiple damages occur at arbitrary locations close to each other, the proposed methodology would likely identify this as a single larger damage.
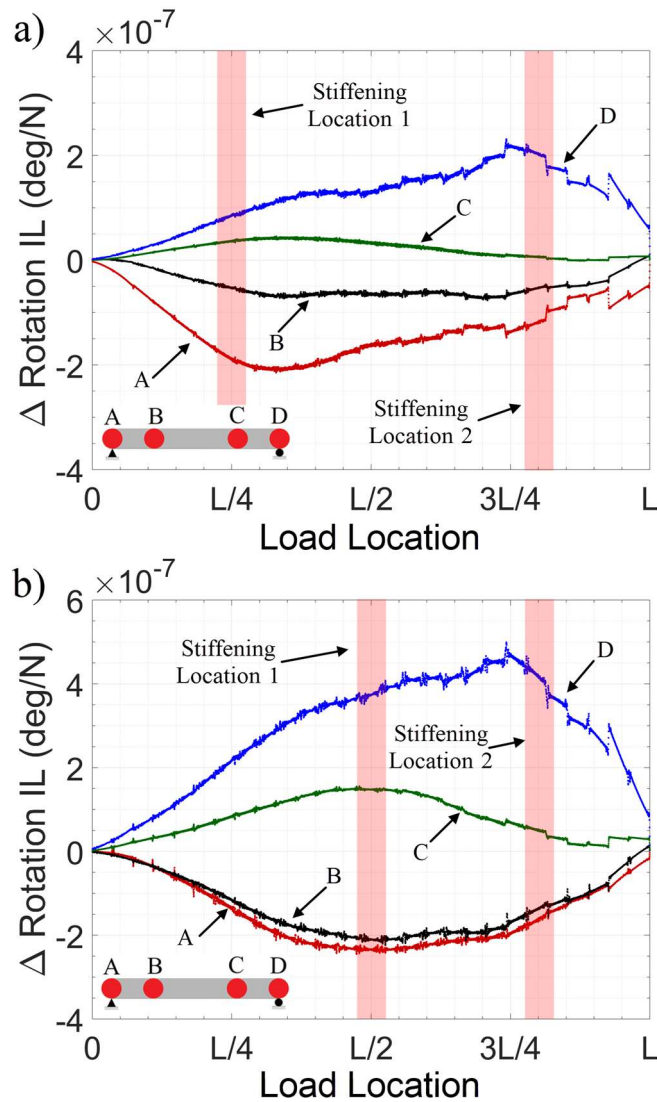
44

Figure 21. Difference in rotation influence line plots for stiffening at multiple locations (refer to Table 4). (a) Multiple Stiffening Case 1 (b) Multiple Stiffening Case 2

Overall, the damage detection results presented above demonstrate that the difference in rotation influence lines (IL) of the model bridge for healthy and damaged states provides an indication of both the magnitude and location of damage. However, it should be noted that, unlike the model bridge tested in this study, in a real bridge of significant width with several parallel longitudinal beams, there will be load sharing in the transverse direction. This will make it more challenging to detect damage in any

45

beams as load is likely to be redistributed when damage takes place. Another important factor affecting the damage detection results is the speed of a traversing vehicle. A vehicle travelling at approximately 20 m/s (~ 70 km/hr) would cross a 20 m bridge in about one second. In the experimental study the vehicle model travelled across the bridge model at the maximum allowable speed limit for the facility (i.e. 1.05 m/s) and took approximately 6 seconds to cross the structure. For future research, the authors recommend further investigation of the capability of the proposed methodology on full scale bridges under more realistic conditions and with realistic measurement windows. However, it should be noted that the sampling frequency of most of the commercially available inclinometers accurate enough to capture the effect of damage occurring in a bridge is around 10 Hz (see Table 1). The response of a 20 m long bridge to a vehicle travelling at high speeds (i.e. 70 km/h) measured using such sensing equipment would result in only 10 data points which is not adequate to construct the accurate influence line of the structure. In this study data acquisition was carried out at high scanning rates (i.e. 512 Hz) hence the instrumentation presented is a promising tool for further investigation of the proposed methodology under more realistic conditions.

6   Conclusions

In this paper a novel bridge condition monitoring methodology using rotation measurements is presented. Initially, numerical analyses are carried out to investigate the concept of identifying damage in bridges using rotation measurements and sensitivity of rotation to damage. These static analyses are carried out on 1-D bridge model loaded with a moving vehicle. As a result of this study, the rotation influence line difference between healthy and damaged bridge states is proposed as a damage indicator. Subsequently, extensive laboratory experiments were conducted on a 5.4 m long simply supported bridge structure, loaded with a multi-axle moving vehicle to validate the findings from the numerical study. The test bridge was instrumented with rotation sensors and axle detectors. It was damaged negatively, i.e., locally stiffened, by clamping steel plates to the deck. A wide range of negative damage scenarios are investigated, including 27 single- and two multiple-damage scenarios applied with different locations of damage along its length. It is demonstrated that, when damage occurs, it results in an increase in the amplitude of rotation measurements, proving that rotation is sensitive to damage.

The rotation response to a moving vehicle of known weight and axle configuration is transformed to calculate the rotation influence lines (IL) for the healthy and damaged states. Damage is identified for each test scenario by subtracting the calculated rotation influence line from the healthy one. Results show that when damage occurs, the plot of difference in rotation influence lines has peaks corresponding to the damage locations. The sensitivity of the sensor to damage depends on its location. It is shown through both numerical and experimental studies that, for a simply supported bridge, the optimum rotation sensor locations, for identifying damage are the supports. When damage was applied at midspan the sensors placed at both supports successfully identified damage. When it was off-centre, the sensor at the support closer to the damage location was best

47

in identifying damage. When damage is at midspan the proposed methodology accurately identifies its location. However, when damage is off-centre, the predicted location is slightly offset from the actual damage location.

It is concluded from this study that:

- Rotation can be accurately measured using an accelerometer and is a sensitive parameter for identifying damage in a bridge. In essence, when damage occurs, it results in an increase in the amplitude of rotation.
- Deriving the rotation influence line is an effective means of separating the contributions to the response of each axle to the passing vehicle.
- It is shown using both numerical and experimental studies that for a simply supported bridge structure, the optimum sensor locations for identifying local damage are the supports
- The difference in the rotation influence line between healthy and damaged bridge states is an effective indication of local damage in a bridge. It provides an indication of both the magnitude and location of damage in laboratory conditions.

Acknowledgements

References

[1] *RAC Foundation Report: Bridge Maintenance in Great Britain in 2016-2017.* 2018.

[2] Rytter A. *Vibration based inspection of civil engineering structures*. Department of Building Technology and Structural Engineering, Aalborg University, Denmark, 1993.

[3] Zhu XQ, Law SS. Wavelet-based crack identification of bridge beam from operational deflection time history. *Int J Solids Struct* 2006; 43: 2299–2317.

[4] Zhang WW, Wang ZH, Ma HW. Studies on Wavelet Packet-Based Crack Detection for a Beam under the Moving Load. *Key Eng Mater* 2009; 413–414: 285–290.

[5] Hester D, González A. A wavelet-based damage detection algorithm based on bridge acceleration response to a vehicle. *Mech Syst Signal Process* 2012; 28: 145–166.

[6] Bradley M, González A, Hester D. Analysis of the structural response to a moving load using empirical mode decomposition. London: Taylor & Francis, pp. 117–117.

[7] Huang NE, Huang K, Chiang W-L. HHT based bridge structural health-monitoring method. In: *Hilbert-Huang Transform and Its Applications*. WORLD SCIENTIFIC, pp. 263–287.

[8] González A, Hester D. An investigation into the acceleration response of a damaged beam-type structure to a moving force. *J Sound Vib* 2013; 332: 3201–3217.

[9]   He W, Zhu S. Moving load-induced response of damaged beam and its application in damage localization. *J Vib Control* 2016; 22: 3601–3617.

[10]   OBrien E, Carey C, Keenahan J. Bridge damage detection using ambient traffic and moving force identification. *Struct Control Heal Monit* 2015; 22: 1396–1407.

[11]   Li ZH, Au FTK. Damage Detection of a Continuous Bridge from Response of a Moving Vehicle. *Shock Vib* 2014; 2014: 1–7.

[12]   Park J, Moon D-S, Spencer BF, et al. Neutral-axis Identification using strain and acceleration measurements. In: *The 2017 World Congress on Advances in Structural Engineering and Mechanics (ASEM17)*. Seoul, Korea, 2017.

[13]   Sigurdardottir DH, Glisic B. Neutral axis as damage sensitive feature. *Smart Mater Struct* 2013; 22: 075030.

[14]   Sigurdardottir DH, Glisic B. Detecting minute damage in beam-like structures using the neutral axis location. *Smart Mater Struct* 2014; 23: 125042.

[15]   Sigurdardottir DH, Glisic B. The neutral axis location for structural health monitoring: an overview. *J Civ Struct Heal Monit* 2015; 5: 703–713.

[16]   Chen Z, Zhu S, Xu Y, et al. Damage Detection in Long Suspension Bridges Using Stress Influence Lines. *J Bridg Eng* 2015; 20: 05014013.

[17]   Chang C-I, Tsai M-H, Liu Y-C, et al. Design and implementation of an extremely large proof-mass CMOS-MEMS capacitive tilt sensor for sensitivity and resolution improvement. In: *2011 16th International Solid-State Sensors, Actuators and Microsystems Conference*. IEEE, pp. 1104–1107.

[18] Liu S, Zhu R. Micromachined Fluid Inertial Sensors. *Sensors (Basel)*; 17. Epub ahead of print 14 February 2017. DOI: 10.3390/s17020367.

[19] Crescini D, Marioli D, Romani M, et al. An inclinometer based on free convective motion of a heated air mass. In: *ISA/IEEE Sensors for Industry Conference, 2004. Proceedings the*. IEEE, pp. 11–15.

[20] Fuxue Zhang. The accelerometer and tilt sensor based on natural convection gas pendulum. In: *International Conference on Information Acquisition, 2004. Proceedings.* IEEE, pp. 122–125.

[21] Weiguan Zhang, Haoshen Zhu, Lee JE-Y. Piezoresistive Transduction in a Double-Ended Tuning Fork SOI MEMS Resonator for Enhanced Linear Electrical Performance. *IEEE Trans Electron Devices* 2015; 62: 1596–1602.

[22] Zhao L, Yeatman EM. Micro Capacitive Tilt Sensor for Human Body Movement Detection. In: *4th International Workshop on Wearable and Implantable Body Sensor Networks (BSN 2007)*. Berlin, Heidelberg: Springer Berlin Heidelberg, pp. 195–200.

[23] Olaru R, Dragoi DD. Inductive tilt sensor with magnets and magnetic fluid. *Sensors Actuators A Phys* 2005; 120: 424–428.

[24] Olaru R, Cotae C. Tilt sensor with magnetic liquid. *Sensors Actuators A Phys* 1997; 59: 133–135.

[25] Antunes PFC, Marques CA, Varum H, et al. Biaxial Optical Accelerometer and High-Angle Inclinometer With Temperature and Cross-Axis Insensitivity. *IEEE Sens J* 2012; 12: 2399–2406.

[26] Frazão O, Falate R, Fabris JL, et al. Optical inclinometer based on a single long-

period fiber grating combined with a fused taper. *Opt Lett* 2006; 31: 2960.

[27]   Wu C-M, Chuang Y-T. Roll angular displacement measurement system with microradian accuracy. *Sensors Actuators A Phys* 2004; 116: 145–149.

[28]   Wyler AG. Levelmatic 31 - High precision analog inclination sensor technical specification, www.wylerag.com (2016).

[29]   Bruns DG. An optically referenced inclinometer with sub-microradian repeatability. *Rev Sci Instrum* 2017; 88: 115111.

[30]   Inaudi D, Glisic B. Interferometric inclinometer for structural monitoring. In: *2002 15th Optical Fiber Sensors Conference Technical Digest. OFS 2002(Cat. No.02EX533)*. IEEE, pp. 391–394.

[31]   Glišić B, Posenato D, Inaudi D, et al. Structural health monitoring method for curved concrete bridge box girders. In: Tomizuka M (ed). International Society for Optics and Photonics, p. 693204.

[32]   Bas S, Apaydin NM, Ilki A, et al. Structural health monitoring system of the long-span bridges in Turkey. *Struct Infrastruct Eng* 2018; 14: 425–444.

[33]   Ko JM, Ni YQ. Technology developments in structural health monitoring of large-scale bridges. *Eng Struct* 2005; 27: 1715–1725.

[34]   Li H, Ou J. The state of the art in structural health monitoring of cable-stayed bridges. *J Civ Struct Heal Monit* 2016; 6: 43–67.

[35]   Andersen JE, Enckell M, Alcover IF, et al. The Structural Health Monitoring System of the Izmit Bay Bridge : overview and SHM-based fatigue assessment. In: *Second Conference on Smart Monitoring, Assessment and Rehabilitation of*

Civil Structures. Istanbul, 2013.

[36]   Haritos N, Chalko TJ. Determination of abutment support conditions in an 80-year-old RC bridge. In: Chase SB (ed) *Proc. SPIE 2946, Nondestructive Evaluation of Bridges and Highways*. International Society for Optics and Photonics, pp. 312–323.

[37]   Hoult NA, Fidler PRA, Hill PG, et al. Long-Term Wireless Structural Health Monitoring of the Ferriby Road Bridge. *Journal of Bridge Engineering* 2010; 15: 153–159.

[38]   Stajano F, Hoult N, Wassell I, et al. Smart bridges, smart tunnels: Transforming wireless sensor networks from research prototypes into robust engineering infrastructure. *Ad Hoc Networks* 2010; 8: 872–888.

[39]   O'Leary P, Harker M. A Framework for the Evaluation of Inclinometer Data in the Measurement of Structures. *IEEE Trans Instrum Meas* 2012; 61: 1237–1251.

[40]   BURDET O, ZANELLA J-L. Automatic Monitoring of Bridges using Electronic Inclinometers. *IABSE Congr Rep* 2000; 16: 1574–1581.

[41]   Hou X, Yang X, Huang Q. Using Inclinometers to Measure Bridge Deflection. *J Bridg Eng* 2005; 10: 564–569.

[42]   He X, Yang X, Zhao L. Application of Inclinometer in Arch Bridge Dynamic Deflection Measurement. *Indones J Electr Eng Comput Sci* 2014; 12: 3331–3337.

[43]   LLoret S, Inaudi D, Vurpillot S. Static and dynamic bridge monitoring with fiber optic sensors. In: Huang S, Bennett KD, Jackson DA (eds) *Proc. SPIE 3555, Optical and Fiber Optic Sensor Systems*. International Society for Optics and

Photonics, pp. 136–146.

[44]   Perregaux N, Vurpillot S, Inaudi D, et al. Vertical Displacement of Bridges using the SOFO System a Fiber Optic Monitoring Method for Structures. In: *12th Eng. Mech. Conference "A Force for the 21st Century", 17-20.05.1998*, pp. 17–20.

[45]   Vurpillot S, Krueger G, Benouaich D, et al. Vertical Deflection of a Pre-Stressed Concrete Bridge Obtained Using Deformation Sensors and Inclinometer Measurements. *ACI Struct J*; 95. Epub ahead of print 1998. DOI: 10.14359/566.

[46]   Robert-Nicoud Y, Raphael B, Burdet O, et al. Model Identification of Bridges Using Measurement Data. *Comput Civ Infrastruct Eng* 2005; 20: 118–131.

[47]   Sousa H, Cavadas F, Henriques A, et al. Bridge deflection evaluation using strain and rotation measurements. *Smart Struct Syst* 2013; 11: 365–386.

[48]   Helmi K, Taylor T, Zarafshan A, et al. Reference free method for real time monitoring of bridge deflections. *Eng Struct* 2015; 103: 116–124.

[49]   Chen J, Qu S, Hou X. The application of inclinometer in natural characteristics testing of beam bridges. In: *The 14th World Conference on Earthquake Engineering*. Beijing, China, http://www.14wcee.org/Proceedings/files/05-02-0019.PDF (2008, accessed 15 April 2018).

[50]   Heng Z, Shu-Ying Q, Guo-Liang W. *Research on the Method of Simply Supported Beam Modal Parameters Recognition by QY Iinclinometer*. Epub ahead of print 30 November 2014. DOI: 10.3923/jas.2014.1844.1850.

[51]   Alten K, Ralbovsky M, Vorwagner A, et al. Evaluation of Different Monitoring Techniques During Damage Infliction on Structures. *Procedia Eng* 2017; 199: 1840–1845.

55

[52] Erdenebat D, Waldmann D, Scherbaum F, et al. The Deformation Area Difference (DAD) method for condition assessment of reinforced structures. *Eng Struct* 2018; 155: 315–329.

[53] Moses F. Weigh-in-Motion System Using Instrumented Bridges. *Transp Eng J ASCE* 1979; 105: 233–249.

[54] McNulty P, O'Brien E. Testing of Bridge Weigh-In-Motion System in a Sub-Arctic Climate. *J Test Eval* 2003; 31: 11686.

[55] OBrien EJ, Quilligan MJ, Karoumi R. Calculating an influence line from direct measurements. *Proc Inst Civ Eng - Bridg Eng* 2006; 159: 31–34.

[56] Yamaguchi E, Kawamura S, Matuso K, et al. Bridge-Weigh-In-Motion by Two-Span Continuous Bridge with Skew and Heavy-Truck Flow in Fukuoka Area, Japan. *Adv Struct Eng* 2009; 12: 115–125.

[57] Huseynov F. *Bridge Condition Assessment Methods Using Rotation Measurements*. University College Dublin, 2019.

[58] International Standards Organisation. *ISO 8608 - Mechanical vibration -- Road surface profiles -- Reporting of measured data*. ISO - International Organisation for Standardization, 2016.

[59] Hester D, Brownjohn J, Bocian M, et al. Low cost bridge load test: Calculating bridge displacement from acceleration for load assessment calculations. *Eng Struct* 2017; 143: 358–374.

[60] Hester D, Brownjohn JMW, Bocian M, et al. Using inertial measurement units originally developed for biomechanics for modal testing of civil engineering structures. *Mech Syst Signal Process* 2018; 104: 776–798.

56

[61] Faulkner K, Huseynov F, Brownjohn J, et al. Deformation Monitoring of a Simply Supported Railway Bridge under Varying Dynamic Load. In: *9th International Conference on Bridge Maintenance, Safety and Management.* Melbourne, Australia, 2018.